Atmos. Chem. Phys., 25, 16451–16477, 2025
https://doi.org/10.5194/acp-25-16451-2025

Atmospheric Chemistry and Physics
Open Access
EGU

Research article

The ACCESS-AM2 climate model underestimates aerosol concentration in the Southern Ocean; improving aerosol representation could be problematic for the global energy balance

Sonya L. Fiddes[1], Matthew T. Woodhouse[2,1], Marc D. Mallet[1], Liam J. Lamprey[1], Ruhi S. Humphries[2,1], Alain Protat[3,1], Simon P. Alexander[4,1], Hakase Hayashida[5], Samuel Putland[6], Branka Miljevic[6], and Robyn Schofield[7]

[1]Australian Antarctic Program Partnership, Institute for Marine and Antarctic Studies, University of Tasmania, Hobart, Australia
[2]CSIRO Environment, Aspendale, Australia
[3]Bureau of Meteorology, Melbourne, Australia
[4]Australian Antarctic Division, Hobart, Australia
[5]Application Laboratory, Japan Agency for Marine-Earth Science and Technology, Yokohama, Japan
[6]School of Earth and Atmospheric Sciences, Queensland University of Technology, Brisbane, Queensland, Australia
[7]School of Geography, Earth and Atmospheric Sciences, University of Melbourne, Melbourne, Victoria, Australia

Correspondence: Sonya L. Fiddes (sonya.fiddes@utas.edu.au)

Received: 6 October 2024 – Discussion started: 21 October 2024
Revised: 22 September 2025 – Accepted: 1 October 2025 – Published: 24 November 2025

Abstract. The interaction of natural marine aerosol with clouds and radiation is a significant source of climate model uncertainty. The Southern Ocean represents a key area to understand these interactions, and a region where significant model biases exist. Here we provide an evaluation of the Australian Community Climate and Earth System Simulator atmosphere model which includes a double-moment aerosol scheme. We evaluate against measurements of condensation nuclei (N10) and cloud condensation nuclei (CCN) number from seven ship campaigns and three terrestrial locations, spanning the years 2015–2019. We find that N10 is heavily underestimated in the model across all regions and seasons by more than 50 % and in some cases by over 80 % at higher latitudes. CCN is also strongly underestimated over marine and Antarctic regions, often by more than 50 %. We then perform seven sensitivity tests to explore different aerosol configurations. We find that updating the dimethyl sulfide climatology and turning on the primary marine organic aerosol flux marginally improves marine CCN by between 4 %–9 %. N10 was reduced by between 3 %–9 %. The Southern Ocean radiative bias is also reduced by this combination of changes, with limited adverse effects. We also test altering the sea spray flux to use wind gust instead of mean wind speed. This significantly improved CCN in the marine regions, but resulted in detrimental impacts on the region's radiation budget, indicating that drastically improving the Southern Ocean's CCN budget may lead to poorer simulations of the global climate.

Published by Copernicus Publications on behalf of the European Geosciences Union.

1 Introduction

Atmospheric aerosol have an important effect on radiation, cloud and precipitation processes that make them an influential component of the Earth's climate. Aerosols affect the Earth's energy budget directly by scattering and absorbing incoming solar radiation, resulting in a cooling effect (McCormick and Ludwig, 1967). Aerosol can also affect the Earth's energy budget indirectly by acting as cloud condensation nuclei (CCN) which enable cloud droplet formation and influence the clouds reflectivity (albedo) and absorption of radiation (Twomey, 1974; Albrecht, 1989; Pincus and Baker, 1994). The ocean surface acts as an important source of natural aerosol to the atmosphere, producing sea spray aerosol (SSA) which is made up by both primary marine organic (PMO) aerosol and sea salts, as well as secondary aerosols derived primarily from the oxidation of dimethyl sulfide (DMS).

Aerosol-cloud-radiation interactions, and how they are modelled, are one of the largest uncertainties in estimates of climate forcing (Boucher et al., 2013; Forster et al., 2023; Watson-Parris and Smith, 2022). A significant contribution to the uncertainty in indirect aerosol-radiative forcing is due to aerosol from natural sources (Carslaw et al., 2013; Regayre et al., 2020). In the Southern Hemisphere, the Southern Ocean has been a key place of interest to study these uncertainties (e.g. see McFarquhar et al., 2021; Schmale et al., 2019), in part due to its remote and relatively untouched environment (Mallet et al., 2023), and in part due to significant radiative biases and uncertainty in climate sensitivity that exist in climate and weather models for the region (Bodas-Salcedo et al., 2014; Protat et al., 2017; Schuddeboom and McDonald, 2021; Regayre et al., 2020; Zelinka et al., 2020). The radiative biases have been attributed to a poor representation of clouds in models. In particular, most models incorrectly or inadequately simulate ice nucleating particle (INP) processes, which results in models overpredicting ice cloud, and underpredicting super-cooled liquid water clouds (Vergara-Temprado et al., 2018; Vignon et al., 2021).

Poor model representation of emission, aerosol mass, size distribution and composition of sea spray aerosol (SSA) contribute to the uncertainty in natural aerosol (De Leeuw et al., 2011). Both Revell et al. (2021) and Paulot et al. (2020) have demonstrated the influence of SSA on the Earth's climate including on the equilibrium climate sensitivity. However, there is much conflicting literature surrounding the parameterisation of SSA, especially over southern high latitudes, making it difficult to truly trust current results in large-scale modelling. For example, Hartery et al. (2020), Venugopal et al. (2025) and Jaeglé et al. (2011) found that the Gong (2003) SSA flux parameterization over-predicted summertime emissions of SSA, and suggested a reduction of the flux for Southern Ocean conditions. In implementing the Hartery et al. (2020) revised parameterisation into a global climate model Revell et al. (2019) found that reducing the sea spray emissions improved wintertime aerosol optical depth, but adverse effects were found for the summertime. On the other hand, using perturbed parameter ensembles and Southern Ocean aerosol observations, Regayre et al. (2020) found that the SSA flux needed to be scaled up by a factor of 3 (or between 1.6–5.1) to reflect the observed aerosol concentrations. This finding opposes the aforementioned studies showing the SSA is overestimated in models, but is a simple way to increase overall aerosol burden. However, a simple scaling can lack the nuance of more physically driven model changes, especially over different regions and seasons.

SSA flux characterisations rely on wind speed with some studies also taking into account the sea surface temperature (SST) (Grythe et al., 2014). In most SSA parameterisations that consider SSTs, the SSA flux increases with increased SSTs, resulting in lower SSA fluxes at high latitudes for equivalent wind speeds. However, the majority of the studies that have deduced these relationships have had very little high latitude data to form comprehensive statistical relationships (e.g. Jaeglé et al., 2011, uses just one voyage in the high latitudes of the Southern Ocean). More recently Sellegri et al. (2023) has suggested that the assumption of the positive SST/SSA relationship may not hold true for the high latitudes of the Southern Ocean, and that this relationship may be modulated by biological activity.

While the uncertainties of SSA fluxes are large when considering the contribution to sea salt aerosol, a further uncertainty is the contribution of PMO mass from biological activity in the ocean (McCluskey et al., 2017, 2018), which is often modelled as a fraction of the total SSA flux. This flux is often not included in aerosol schemes. As well as contributing to the overall aerosol mass and number, PMO play an important role as a source of INP (McCluskey et al., 2017), which again, are often not accounted for (Burrows et al., 2022).

Global surface seawater concentrations and emission of DMS are considered the second largest source of uncertainty with respect to natural aerosol emissions (Carslaw et al., 2013). In many climate models, DMS is represented by a fixed monthly climatology, based on spatially and temporally biased observations resulting in the climate effects of DMS being poorly understood and poorly captured by climate models (Quinn and Bates, 2011; Fiddes et al., 2018; Bhatti et al., 2023). While a new climatology has been released (Hulswar et al., 2022), online DMS produced by ocean biogeochemical models is desirable to represent variability in the DMS emissions (Bock et al., 2021). Other climatologies developed from satellite records or machine learning also offer potential alternatives to the observational derived climatologies (Wang et al., 2020; Galí et al., 2018) including to provide time-varying data sets as done in Zhou et al. (2024). Uncertainty around the flux parameterisation also remains, though much literature is now recommending linear parameterisations (e.g. Liss and Merlivat, 1986), which provides

a lower emission compared to other methods (Vlahos and Monahan, 2009; Bell et al., 2017; Bhatti et al., 2023).

Not only are the sources of aerosol and their precursors poorly captured in climate models, but the subsequent atmospheric processes they are involved in also contain significant uncertainty. New particle formation (NPF) is frequently observed in the free troposphere (Curtius, 2006; McCoy et al., 2021), though is more rarely detected in the marine boundary layer (BL) (Modini et al., 2009; Brean et al., 2021; Schmale et al., 2019). In a modelling study, Merikanto et al. (2009) estimated 45 % of CCN at a 0.2 % supersaturation were secondary aerosol formed through nucleation. Within the marine BL, nucleation accounts for 55 % of CCN (0.2 %) of which 45 % were transported from the free troposphere to the marine BL and 10 % are formed in the marine BL (Merikanto et al., 2009). Nucleation processes include binary nucleation between sulfuric acid and water (Kulmala et al., 1998), ternary nucleation between sulfuric acid, water and ammonia (Korhonen et al., 1999) and ion-induced nucleation between highly oxidised biogenic vapours (Kirkby et al., 2016). However, parameterisations of NPF are often limited to only binary nucleation. Other biogenic vapours aside from DMS have also been found to nucleate and are suggested as an important source of CCN in the pre-industrial period (Gordon et al., 2016), but are often neglected in models. Additionally, marine volatile organic compounds (VOCs), such as isoprene, can reduce the atmospheric oxidative capacity by reacting with OH (as well as O_3 and NO_3 to a lesser degree) in the troposphere. Such VOCs can also yield secondary organic aerosol and provide condensational mass, further influencing the clouds and climate. In the case of marine isoprene, this occurs on a much smaller scale than that of DMS (Yu and Li, 2021), with isoprene concentrations being very low outside of phytoplankton blooms and biologically active coastal regions of the Southern Ocean (Ferracci et al., 2024).

Aerosol sinks, and how they are modelled, are also a key source of uncertainty. Aerosol can be removed from the atmosphere via dry deposition or wet deposition. Dry deposition is difficult to measure and evaluate. Regayre et al. (2020) after applying Southern Ocean observational constraints to a perturbed parameter ensemble, find that it is likely that a scaling factor for the accumulation mode dry deposition velocity in the Unified Model needs to be lower than the default value resulting in a reduced sink of aerosol. Other observational studies have indicated that wet deposition (rain after coalescence of cloud droplets) is an important control of CCN variability in the Southern Ocean, particularly in relation to shallow convection (Alinejadtabrizi et al., 2024) and stratocumulus (Kang et al., 2022). Given the tendency for models to produce too much light rain (Stephens et al., 2010), it has been suggested that wet deposition may be overestimated in models (Kang et al., 2025).

Representative aerosol observations are essential for evaluating and constraining aerosol simulations produced by climate models (Regayre et al., 2020; Mallet et al., 2023). Appropriate datasets are few in the Southern Hemisphere relative to the Northern Hemisphere, which has added to the difficulty of modelling this region. Recent field campaigns have focused on collecting measurements of aerosol, cloud, precipitation and radiation properties, including vessel and land-based campaigns around Australia and the Southern Ocean (McFarquhar et al., 2021; Schmale et al., 2019), and measurements collected from long term monitoring stations (Gras and Keywood, 2017; Hara, 2023). Importantly, these campaigns have identified seasonal and latitudinal trends in aerosol, as well as detecting distinct continental (both Antarctic and Australian) and free-tropospheric influence on marine air masses (Humphries et al., 2021a; Alroe et al., 2020; Simmons et al., 2021; Gras and Keywood, 2017; McFarquhar et al., 2021; Schmale et al., 2019; Mallet et al., 2025). While there have been a number of modelling studies that have focused on one or two campaigns in detail (e.g. Regayre et al., 2020; McCluskey et al., 2023; Revell et al., 2019) there has been no model evaluation of aerosol concentrations for the Southern Ocean/Antarctic that considers a latitudinal and seasonal perspective. The recent suite of campaign data presented by Humphries et al. (2023) provides the perfect opportunity for such an analysis.

In this work, we evaluate the performance of the Australian Community Climate and Earth System Simulator – atmosphere model (ACCESS-AM2), which includes the Global Model of Aerosol Processes (GLOMAP)-mode aerosol scheme, in simulating CCN and condensation nuclei (particles with a dry diameter greater than 10 nm – N10) using vessel and station-based observations in the Australian Antarctic region and Southern Ocean. We further perform a series of experiments where we change the aerosol formation from SSA, PMO, DMS and BL NPF to evaluate how these may affect Southern Ocean and Antarctic aerosol populations. By performing these evaluations of N10 and CCN, we can gain a better understanding of the modelled aerosol population and its biases. Examining the population at two different sizes can give us insight as to how different species may impact both the overall aerosol population as well as that of cloud-relevant size and the growth that occurs to this size. With this knowledge, we can outline how the model biases associated with aerosol-cloud-radiation interactions around the Southern Ocean and Antarctic can be better understood and the degree of uncertainty reduced.

2 Data and Methods

2.1 ACCESS-AM2

The ACCESS-coupled model (ACCESS-CM2 Bi et al., 2020) is an Australian coupled climate model which can be run in an atmosphere-only mode (ACCESS-AM2 Bodman et al., 2020). The ACCESS-AM2 model is configured for the Coupled Model Inter-comparison Project phase 6 CMIP6 (Eyring et al., 2016) Atmospheric Model

Inter-comparison Project (AMIP). Importantly, ACCESS-CM2 and ACCESS-AM2 include the modal aerosol module Global Model of Aerosol Processes (GLOMAP-mode) (Mann et al., 2010, 2012), which we will describe shortly.

A description of the specific simulation set-up used in this work can be found in (Fiddes et al., 2022). Briefly, ACCESS-AM2 uses the UK Met Office's Unified Model Global Atmosphere (UM10.6 GA7.1) as the atmospheric module, the Community Atmosphere Biosphere Land Exchange model version 2.5 (CABLE2.5) as the land-surface module while aerosol and related processes are simulated by GLOMAP-mode (Bi et al., 2020). ACCESS-AM2 is configured with a horizontal resolution of 1.25° latitude and 1.875° longitude, has 85 vertical levels, with 50 levels below 15 km and 35 levels above reaching a top height of 85 km. The model has been run for the years 2014–2019 (with 2014 discarded as a spin up year), with daily means as the output.

The ACCESS-AM2 model has been configured for the CMIP6 AMIP experiment which uses CMIP6 forcings for monthly sea surface temperature (SST), sea ice concentrations (SIC), solar forcing, greenhouse gases (GHGs), volcanic aerosol optical depth, aerosol chemistry and ozone (Eyring et al., 2016). The shared socioeconomic pathway (SSP2-4.5), a middle of the road scenario using emissions described in Feng et al. (2020), was used post-2014 (Fricko et al., 2017; Gidden et al., 2019). The simulations here have been nudged to the European Centre for Medium-Range Weather Forecasts Reanalysis 5th Generation (ERA5 Hersbach et al., 2020) for horizontal wind speed and potential temperature in the free troposphere at three hourly intervals.

The Community Emissions Data System (CEDS) provided historical (for 2014 – our spin up year) data for anthropogenic emissions of chemically reactive gases, carbonaceous aerosol and CO_2 (Horsley et al., 2018). Historical global emissions from biomass burning were provided by the Global Fire Emissions Database version 4 with small fires (GFED4s) (Van Marle et al., 2017).

GLOMAP-mode

GLOMAP-mode is a comprehensive, two moment, pseudo-modal aerosol scheme. A detailed description of the GLOMAP-mode module is provided in Mann et al. (2010), and Mann et al. (2012). GLOMAP-mode includes sulfate, sea salt, black carbon and organic matter, distributed across five internally mixed modes: soluble nucleation, Aitken, accumulation and coarse modes, and the insoluble Aitken mode (Mann et al., 2010). GLOMAP-mode simulates aerosol in a size-resolved manner and includes primary emission and secondary formation, growth by condensation and coagulation, cloud processing and removal by dry deposition and scavenging (wet deposition) (Mann et al., 2010).

For this work, the DMS emission flux from the ocean to the atmosphere is calculated using the surface water DMS climatology outlined in Kettle et al. (1999). The oldest DMS climatology was used in error in the released version of the model (Bi et al., 2020), however the majority of experiments in this study will be evaluated using the Lana et al. (2011) climatology in line with the GA7.1 configuration (Walters et al., 2019). The DMS flux parameterisation is provided by Liss and Merlivat (1986). Further description and discussion about the uncertainties of DMS climatologies and flux parameters can be found in Fiddes et al. (2018) and more recently in Bhatti et al. (2023). The DMS flux is scaled by a factor of 1.7 to take into account the lack of PMO, which are not switched on by default (Mulcahy et al., 2018). This is different in later versions of GLOMAP-mode, which returns DMS to a scaling of 1 and turns on PMO (Mulcahy et al., 2020). SSA emission fluxes are calculated using the wind-speed parameterization source function developed by Gong (2003), and include the updated sea salt density as per Mulcahy et al. (2020). NPF by the binary homogeneous nucleation of water and sulfuric acid in the free troposphere is parameterised according to Kulmala et al. (1998), while BL NPF is not switched on. Dust emissions are determined externally to GLOMAP-mode using a binning method outlined in Woodward (2001). Other trace gas and primary aerosol emissions from anthropogenic and terrestrial sources include volcanic-sourced and industrial SO_2, biomass burning and monoterpenes. These are prescribed according to CMIP6 protocols (Eyring et al., 2016).

2.2 Experimental simulations

For this study, seven further model simulations were analysed for responses to imposed changes to aerosol formation or sources. The control simulation is setup as per the description in the previous section, while each of the seven experiments varies from this set-up, which is summarised in Table 1. These sensitivity tests range from realistic and established updates through to some experimental-only changes that are hypothesized to improve aerosol. They include tests that bring the model in line with recent UM configurations (e.g. the inclusion of primary marine organics), the use of updated ancillary data (i.e. the new DMS climatology), and examining the applicability of existing parameterisations that are usually not used in this region (i.e. boundary layer new particle formation). Furthermore, changing the sea salt parameterisation and using a model-derived daily updating DMS field are more experimental but are useful for future model development.

2.2.1 BL NPF

In our first experimental simulation, which we refer to as the "BL NPF" simulation, we use the Metzger et al. (2010) BL NPF parameterisation, which involves the organic-mediated nucleation of H_2SO_4 and an organic compound ("NucOrg"). The nucleation rate equation outlined in Metzger et al. (2010) is shown by Eq. (1), where $J_{1.5}$ is the nucleation rate of

Table 1. The eight simulations run to evaluate aerosol concentrations in the Southern Ocean. Each experimental simulation describes a change to the way aerosol are produced but are otherwise the same as the Control (not the Control*).

Simulation	Aerosol configuration	Reference
Control*	As described in Sect. "GLOMAP-mode" using the Kettle et al. (1999) DMS climatology	Mann et al. (2010); Kettle et al. (1999)
Control	As for Control* but with the Lana et al. (2011) DMS climatology	Mann et al. (2010); Lana et al. (2011)
BL NPF	Boundary layer nucleation turned on	Metzger et al. (2010)
SSA gust	Use max wind gust instead of mean wind in the SSA flux	Motivated by Regayre et al. (2020)
PMO	Primary marine organics aerosol emission turned on	Gantt et al. (2012)
H22 DMS	Revision 3 DMS climatology used	Hulswar et al. (2022)
OM2 DMS	Daily DMS derived from ACCESS-Ocean Model (OM) 2	Kiss et al. (2020); Hayashida et al. (2021)
PMO + H22	Combined H22 DMS climatology scaled to 1.0 with PMO switched on	Hulswar et al. (2022); Gantt et al. (2011)

1.5 nm dry diameter stable particles, k is the rate constant, and m and n are the reaction orders for sulfuric acid and the organic compound respectively. In ACCESS-AM2 the organic compound is provided by secondary organic carbon precursors (treated as monoterpenes, noting that GLOMAP-mode does not include isoprene).

$$J_{1.5} = k[\mathrm{H_2SO_4}]^m[\mathrm{NucOrg}]^n \quad (1)$$

2.2.2 SSA emissions

In this experiment, "SSA gust", we increase the SSA flux to better match observed total aerosol concentrations (not SSA aerosol alone), as suggested by Regayre et al. (2020). Instead of applying a factor of three scaling as suggested by Regayre et al. (2020), we have instead substituted the daily mean horizontal wind speed with the daily mean horizontal maximum wind gust at 10 m (u_{mx10}). This reflects the higher wind speeds observed in the Southern Ocean compared to elsewhere, and the fact that over the course of an hour (the model time steps that SSA is calculated), much of the SSA is likely to come from these gusty periods. GLOMAP-mode uses the Gong (2003) parameterisation (Eq. 2) where the size binned flux emission of sea spray $\frac{\mathrm{d}F}{\mathrm{d}r}$ depends on the particle radius at 80 % humidity (r), the horizontal wind at 10 m (u_{10}), and a shape parameter of the size distribution Θ).

$$\frac{\mathrm{d}F}{\mathrm{d}r} = 1.373u_{mx10}^{3.41}r^{-A}(1+0.057r^{3.45}) \times 10^{1.607e^{-B^2}} \quad (2)$$

$$A = 4.7(1+\Theta r)^{-0.017r^{-1.44}} \quad (3)$$

$$B = \frac{(0.433 - \log(r))}{0.433} \quad (4)$$

2.2.3 PMO

The experiment "PMO" switches on PMO aerosol emission, via the SSA function, which currently assumes all aerosol to be salt. This empirical parameterisation (Gantt et al., 2011, 2012) uses the 10 m wind speed (u_{10} in m s^{-1}), ocean chlorophyll-a (CHL in mg m^{-3}) and sea spray particle dry diameter (D_p in µm) to calculate the organic mass fraction ($\mathrm{frac_{OM}}$) of the SSA (Eq. 5). The wind speed function is used here to represent surface tension of the sea surface microlayer (surface accumulation of organics). Higher wind speeds break this layer up, resulting in fewer organics being lofted into the atmosphere. Primary marine organic emissions are positively correlated to the seasonal cycle of CHL, acting as a proxy for biological productivity. The organic fraction of SSA is inversely related to the SSA particle size at submicron scales (the smaller the particle, the more organic fraction), while at super-micron sizes, the organic fraction is small and relativity constant. To calculate the mass flux of organics ($\mathrm{flux_{OM}}$ in g m^{-2} s^{-1}) the fraction of organic material is applied to the volume flux of sea salt aerosol (V_SSA in cm^3 m^{-2} s^{-1}) multiplied by the density of sea spray aerosol particle (ρ_SSA in g cm^{-3}) (Eq. 6). The organic mass flux is then added to the Aitken mode, 25 % to the soluble mode, and 75 % to the insoluble mode (Mulcahy et al., 2020).

$$\mathrm{frac_{OM}} = \frac{\frac{1}{1+\exp(3(-2.63\mathrm{CHL})+3(0.18(u_{10})))}}{1+0.03\exp(6.81D_\mathrm{p})} + \frac{0.03}{1+\exp(3(-2.63\mathrm{CHL})+3(0.18(u_{10})))} \quad (5)$$

$$\mathrm{flux_{OM}} = \mathrm{frac_{OM}} \times V_\mathrm{SSA} \times \rho_\mathrm{SSA} \quad (6)$$

The default DMS emissions remain at the 1.7 scaling in this simulation. We have tested reducing the the DMS emissions scaling to 1.0 with the PMO switched on in a further simulation in combination with the new DMS climatology described below.

2.2.4 DMS climatologies

The Control* simulation uses the original Kettle et al. (1999) DMS climatology, which is used by default in the ACCESS-AM2 model despite the recommendation of using the Lana et al. (2011) climatology, as described in Sect. "GLOMAP-mode". All DMS climatologies are shown by their seasonal means in Fig. 1. Significant literature exists around the production and differences of DMS climatologies and we refer readers to Hulswar et al. (2022), Lana et al. (2011), and Zhou et al. (2024).

The "H22" experiment refers to the use of the Hulswar et al. (2022) DMS climatology. This climatology uses signif-

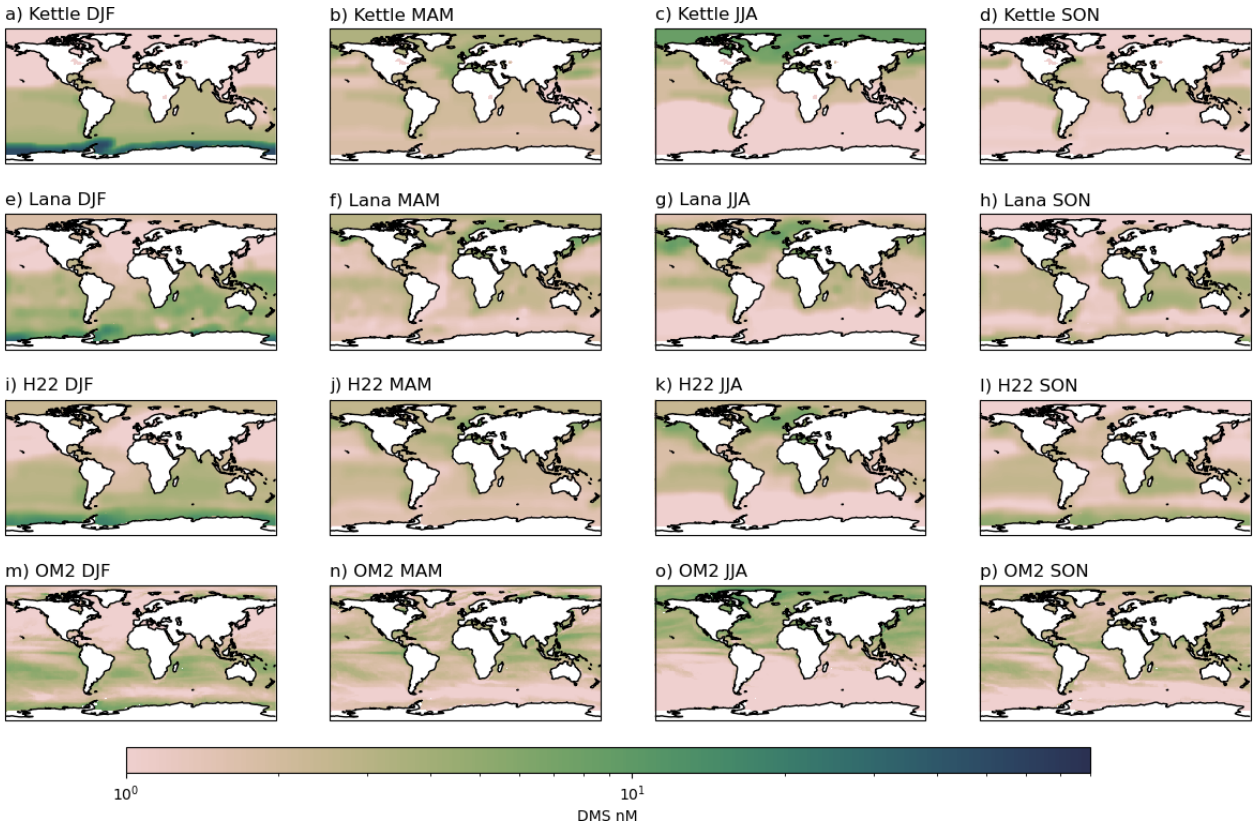

Figure 1. The seasonal mean DMS (nM) climatologies (from left to right DJF, MAM, JJA, SON) for, from top to bottom: Kettle et al. (1999), Lana et al. (2011), Hulswar et al. (2022) and the daily resolving OM2 parameterisation.

icantly updated observations and methodology to account for observational biases, seasonality of biogenic regions and the interpolation of missing data.

We have also produced a daily, annually varying DMS dataset derived from output of the ocean component of ACCESS, ACCESS-OM2. We refer to this experiment as "OM2 DMS". Details of ACCESS-OM2 and the simulation used to produce the DMS output can be found in Kiss et al. (2020) and Sects. 2.1 and 3.1 of Hayashida et al. (2021). ACCESS-OM2, in this case has used the atmospheric boundary conditions from the Control* experiment to drive the model (instead of reanalysis). We highlight that this DMS data set differs from the previous in that it is not a climatology – it is an annually varying dataset at a daily scale, able to respond to atmospheric and oceanic forcings. The benefit of a daily varying dataset is that it is able to respond to atmospheric and oceanic forcings, such as sea surface temperatures or wind speed. This method can present, potentially, a more tightly coupled system, and if the parameterisation is accurate, yield more realistic DMS fields (including DMS in the water and the atmosphere). Some modelling groups are already adopting online DMS production (Bock et al., 2021), so this is a first step towards this goal for ACCESS.

The parameterisation used here to estimate the DMS surface water concentration has been developed for the North Pacific ocean (Aranami and Tsunogai, 2004). Little testing for such parameterisations have been done to this point for the Southern Ocean, in part due to very limited observations. This should be viewed as a starting point for developing online DMS in the ACCESS-OM2 model. Furthermore, as Bhatti et al. (2023) notes, time-varying datasets are preferable over the fixed monthly climatologies given their ability to represent day-to-day fluctuations of the DMS production. The OM2 parameterisation considers two regimes based on the ratio of chlorophyll-*a* concentration (CHL in mg m^{-3}) to the ocean mixed layer depth (MLD in m), as shown in Eq. (7) below from Bock et al. (2021). Chlorophyll-*a* concentrations are diagnosed in ACCESS-OM2 assuming a fixed nitrogen-to-chlorophyll ratio following Oke et al. (2013). Under a low ratio, DMS concentrations depend only on the MLD, where DMS concentrations are considered to be more diluted with greater MLDs. Only under a high ratio, where either high CHL or moderate-low CHL and a shallow MLD, did the authors find that DMS was correlated with CHL, hence necessitating the two conditional equations.

$$\mathrm{DMS} = \begin{cases} \frac{60}{\mathrm{MLD}} & \text{if: } \frac{\mathrm{CHL}}{\mathrm{MLD}} < 0.02 \\ 55.8 \cdot \frac{\mathrm{CHL}}{\mathrm{MLD}} + 0.6 & \text{if: } \frac{\mathrm{CHL}}{\mathrm{MLD}} \geq 0.02 \end{cases} \quad (7)$$

2.3 Field Observations

The ACCESS-AM2 model aerosol scheme was evaluated against a number of observations from field campaigns carried out on research vessels and at land-based research stations. Most of these observations have been described, collated, quality controlled, harmonised and evaluated in Humphries et al. (2023). The Humphries et al. (2023) paper provides the first seasonal and latitudinal description of Southern Ocean aerosol properties, providing an ideal basis from which to perform a modelling evaluation for this region.

A map showing the tracks for vessel-based campaigns and locations of research stations in shown in Fig. 2. Measurements of N10 number concentrations, and CCN concentrations at 0.5 % supersaturation were used as these variables were available for most observation sources. Brief summaries for each of the field campaigns and their respective instruments and operations are provided below, while much greater detail can be found in the Humphries et al. (2023) paper.

2.3.1 Research Vessel Investigator

The Research Vessel Investigator (RVI) is a marine research vessel which has included "underway" (automatic observations taken continuously while the ship is operating) N10 and CCN measurements since 2015. The RVI is also the world's first World Meteorological Organisation Global Atmosphere Watch (WMO GAW) mobile station capable of undertaking continuous atmospheric composition measurements. Aerosol number concentrations (including N10) are measured using a modified condensation particle counter (TSI CPC model 3772, Shoreview, Minnesota, United States) while CCN number concentrations are measured using a CCN counter (CCNC, Model CCN-100, Droplet Measurement Technologies, Longmont, Colorado, United States). The CPC on the Investigator operates at a frequency of 1 Hz which was used to calculate daily medians for the analysis. The CCNC sampled 1 Hz CCN at 1.0 %, 0.6 %, 0.5 %, 0.4 %, 0.3 % and 0.2 % supersaturations sequentially, resulting in 10 min at each setting and the sequence repeated hourly. The atmospheric instruments on the RVI can be affected by exhaust emissions from the ship's engine combustion and waste incineration. The RVI aerosol data therefore must be exhaust filtered using the algorithm described in Humphries et al. (2019), and manually reviewed in order to identify and remove periods when ship exhaust had been sampled.

The observations used in this study have been made during specific atmospheric-focused voyages, after which stringent quality control has been undertaken. These voyages include the Cold Water Trials during January–February 2015; Polar Cell Aerosol Nucleation (PCAN) during January–March 2017; Ice2Equator during April–June 2016; and Clouds, Aerosols, Precipitation, Radiation, and atmospheric Composition Over the southeRn oceaN (CAPRICORN) 1 and CAPRICORN 2 which occurred during March–April 2016 and January–February 2018, respectively. These voyages are described in more detail in Humphries et al. (2023). CCN data is available for all voyages, but N10 data was not available for PCAN, CAPRICORN1 and Ice2Equator. We have limited Ice2Equator data to south of 47.5° S to avoid terrestrial influence from New Zealand.

2.3.2 MARCUS

During the period of October 2017 to March 2018, the Research Survey Vessel Aurora Australis (RSV AA) hosted the Measurements of Aerosol, Radiation and Clouds over the Southern Ocean (MARCUS) campaign. The MARCUS campaign utilised the Atmospheric Radiation Measurement (ARM) project Mobile Facility including the Aerosol Observing System (Uin et al., 2019), which was deployed on the RSV AA to make observations across the Southern Ocean and in sea ice zones as the ship completed resupply voyages between Hobart and the Mawson, Davis, Casey and Macquarie Island stations (McFarquhar et al., 2021). During MARCUS, the Aerosol Observing System collected measurements of aerosol number concentrations using a CPC (TSI CPC model 3772, Shoreview, Minnesota, United States) sampling at a frequency of 1 Hz (Humphries et al., 2021a). A CCN counter (CCNC, Model CCN-100, Droplet Measurement Technologies, Longmont, Colorado, United States) was used to determine CCN concentrations at supersaturations of 0.0 %, 0.1 %, 0.2 %, 0.5 %, 0.8 % and 1.0 % for 10 min each over an hour (Humphries et al., 2021a). Due to the setup of the ARM equipment near the RSV AA exhaust pipe, a majority of the observations were exhaust contaminated and required filtering (Humphries et al., 2021a). The data were exhaust filtered using the exhaust identification algorithm outlined in Humphries et al. (2019), and then manually using air composition data (Humphries et al., 2021a).

2.3.3 CAMMPCAN

In the following summer the RSV AA completed the same re-supply voyages from October 2018 to March 2019 with the Chemical and Mesoscale Mechanisms of Polar Cell Aerosol Nucleation (CAMMPCAN) campaign onboard, including the Atmospheric Integrated Research facility for Boundaries and Oxidative eXperiments (AIRBOX) mobile facility. The CAMMPCAN campaign hosted a CPC (TSI CPC model 3772, Shoreview, Minnesota, United States) sampling at a frequency of 1 Hz, and a CCNC, Model CCN-100, Droplet Measurement Technologies, Longmont, Colorado, United States) to measure CCN concentrations at supersaturations of 0.0 %, 0.1 %, 0.2 %, 0.5 %, 0.8 % and 1.0 % for 10 min each over an hour. Black carbon measurements at 5 min averages were used to initially filter the data for ship exhaust influence, with a threshold value of 70 ng m^{-3} used. Following this, the same exhaust filtering as described

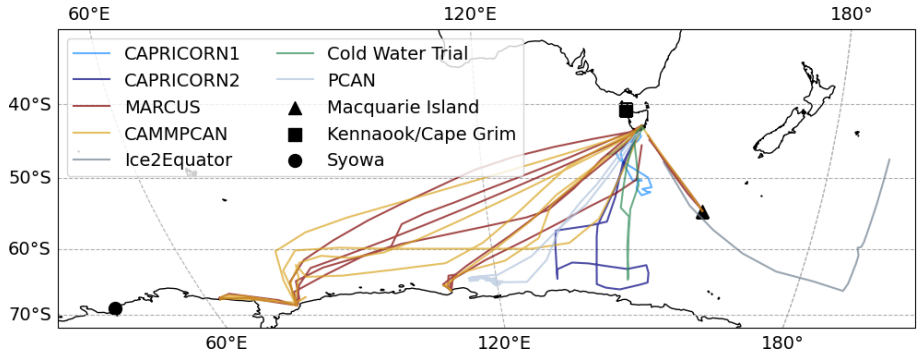

Figure 2. Overview of the field observations used in this work. Blues (CAPRICORN 1 and 2), green (Cold Water Trial) and greys (Ice2Equator and PCAN) shows measurements from campaigns aboard the RV Investigator, red illustrates the MARCUS campaign while yellow shows the CAMMPCAN campaign, both aboard the RSV Aurora Australis. The ship voyage tracks are the daily mean ship location. In black are the locations of the land-based stations of Kennaook/Cape Grim (square), on Tasmania's north-west coast, and Macquarie Island in the middle of the Southern Ocean (triangle) and Syowa (circle) on the Antarctic coast.

in Humphries et al. (2019) were applied to these data. Manual inspection and filtering of the resultant data was then completed using concurrent CO and CO_2 measurements.

2.3.4 Kennaook/Cape Grim

Kennaook/Cape Grim (KCG) is an atmospheric monitoring station located in the northwest of Tasmania (40.7° S, 144.7° E) that has been operating since the mid 1970s (Gras and Keywood, 2017). The KCG station is positioned on a cliff 94 m above the sea level to maximise observations from the Southern Ocean which represents primarily pristine marine air that is mostly unaffected by anthropogenic influences (Gras and Keywood, 2017). Atmospheric particle sampling procedures at KCG generally follow the WMO GAW Aerosol Programme Recommendations (World Meteorological Organization, 2016). Measurements of aerosol number concentrations were made using a set of condensation particle counters (TSI 3760/TSI 3010) running at a frequency of 1 Hz and averaged over minutely intervals (Gras and Keywood, 2017). CCN concentrations primarily at 0.5 % supersaturation were measured using a CCN counter (CCNC, Model CCN-100, Droplet Measurement Technologies, Longmont, Colorado, United States) (Gras and Keywood, 2017). N10 measurements were available for the period 2016–2018 while CCN data was available for 2015–2018. Further station descriptions for KCG are provided in Gras and Keywood (2017). The data presented here is the baseline filtered data (as described in Gras and Keywood, 2017). Baseline air is considered the worlds cleanest air, as unaltered by human activity as physically possible. At KCG, baseline air is identified as air that has come from the Southern Ocean where the wind direction was between 190 and 280° and the radon concentration (a marker of terrestrial influence) is below 100 mBq.

2.3.5 Macquarie Island

Macquarie Island is located at 54.5° S, 158.9° E and is the site of a year-round research station. The position of Macquarie Island in the Southern Ocean makes it a suitable location for monitoring cloud, radiation precipitation and aerosol properties over the region. The Macquarie Island research station hosted the Macquarie Island Cloud and Radiation Experiment (MICRE) which ran from March 2016 to March 2018. Measurements of N10 were made using a modified condensation particle counter (TSI CPC model 3772, Shoreview, Minnesota, United States) at a frequency of 1 Hz which were averaged to hour intervals. A CCN counter (CCNC, Model CCN-100, Droplet Measurement Technologies, Longmont, Colorado, United States) was used was used to determine CCN concentrations at supersaturations of 0.2 %, 0.3 %, 0.4 %, 0.5 %, 0.6 %, 1.0 % each hour. The aerosol measurement set-up is described in Humphries et al. (2023). A campaign report for MICRE is provided in Marchand (2020) and McFarquhar et al. (2021), which includes a summary of the experiment objectives and instruments used.

2.3.6 Syowa

Syowa Station is an Antarctic research station located on East Ongul Island in Lutzow-Holm Bay (69.0° S, 39.0° E). The station is coastal and surrounded by seasonally varying sea-ice year round. A detailed description of Syowa and the station operations is provided in Hara et al. (2011, 2021). The station operates several CPCs (TSI model 3010, Shoreview MN, USA) that have been collecting aerosol measurements since 1997. Measurements of N10 were available as daily means and medians. Measurements of CCN were not available. The Syowa data was included to provide a long term, high latitude record of aerosol number concentrations that could be contrasted with northern and mid-latitude stations

of KCG and Macquarie Island. The data for Syowa is publicly accessible in Hara (2023).

2.4 Analysis methods

2.4.1 Aerosol evaluation

N10 has been chosen for analysis over other size cutoffs given its availability across voyages/stations. The CCN measured at a supersaturation of 0.5 % is the most commonly measured saturation across all campaigns used in this study, allowing for consistent comparison. The model does not provide CCN diagnostics at a specific supersaturation, but provides CCN at selected dry diameters. The modelled size distribution can be used to calculate CCN at any particular activation diameter. To identify an equivalent activation diameter for the 0.5 % supersaturation, we have used the method described in Petters and Kreidenweis (2007) Eq. (10) and Table 1 to identify a suitable hygroscopicity parameter (κ) from which we can calculate the critical activation diameter. We have assumed that the majority of model aerosol is internally mixed H_2SO_4, i.e most aerosol have a coating of H_2SO_4 and therefore, kappa = 0.9. This results in a dry diameter of approximately 40 nm. The mean daily CCN40 particle concentration (aerosol particles with a dry diameter greater than 40 nm) was then calculated from the model size distributions. Our method is in line with assumptions made in previous GLOMAP-mode studies (e.g. Mann et al., 2010). Activation ratios with an externally mixed assumption for the modelled aerosol were also tested, giving an activation diameter of 35 nm, which we believe to be unrealistic for this region (Fossum et al., 2018). The full workflow for these tests can be found in the linked GitHub repository for this work.

The calculation for estimating a critical diameter for a given supersaturation is imperfect and does increase the uncertainty of our results. We have also tested the critical diameter at CCN50 (which more closely matches observed aerosol populations at 0.5 % super saturation Fossum et al., 2018), which showed better results near Kennaook/Cape Grim (no longer overestimated), and marginally worse results elsewhere. However, our critical diameter calculations were consistent in reporting 40 nm as the cut-off for the modelled aerosol size distribution, and hence we have shown only these results.

Aerosol comparisons were performed only on the days in which observational data was available, ensuring a like-for-like comparison (i.e. the datapoints were matched in space and time). The linearly interpolated model gridbox for each location (see Sect. 2.4.2 was used to perform the comparisons. This is also true for KCG, where choosing a gridbox to the south-west of the station, as is normal practice for this location when studying baseline airmasses (which are not influenced by terrestrial air), resulted in poorer performance. This could be due to the fact that moving even one gridbox away diagonally, in a very coarse resolution model, is enough to change the synoptic circulation compared to that experienced at the station. We also recognise that at KCG we have not performed a similar baseline filtering to the model data, in part due to lack of radon in the model (see Sect. 3.3.4 for details). Instead we we have matched the model data to the available daily mean baseline-filtered observations. This may introduce some bias given the coarse resolution of the model, but given the model is nudged to ERA5, we expect the large scale flow to be accurate (Uhe and Thatcher, 2015; Telford et al., 2008).

2.4.2 Data processing

Model data was extracted by linearly interpolating model grid coordinates using the python Xarray library (Hoyer and Hamman, 2017) to the mean daily latitude and longitude locations of the observations. Schutgens et al. (2017) recommend collocating model and observational data at hourly intervals to reduce representation error. However, for these simulations this approach was not feasible. The data was grouped by latitudinal sectors defined in Humphries et al. (2023). The sectors are defined as a northern region ($< 45°$ S), the mid-latitudes (45–60° S), a sub-polar region (60–65° S) and the Polar Cell ($> 65°$ S). Quantitative summaries of all our results can be found in the published code linked to this paper (see Sect. "Code and data availability").

2.4.3 Radiation evaluation

We have used the top of atmosphere outgoing shortwave radiation from the Clouds and the Earth's Radiant Energy System (CERES) Syn1Deg product (Doelling et al., 2013, 2016). More information on this product and its use for this study can be found in Fiddes et al. (2022). The radiation evaluation was carried out for the full 5 year period, as satellite products are also available over this time.

3 ACCESS-AM2 aerosol evaluation and sensitivity testing

In this section we show that the ACCESS-AM2 model strongly underestimates both the N10 and CCN concentrations, which points to issues with the model's ability to accurately represent the aerosol population. The results will be analysed and interpreted together in Sect. 5.

3.1 N10

Figure 3a–c shows the modelled and observed N10 concentration seasonal cycle for KCG, Macquarie Island and Syowa. For KCG, the model underestimates the baseline observations by 53 % on average, with the largest relative underestimations in winter (60 %) and the smallest in autumn (41 %). The control run does appear to capture a seasonal

cycle (see Fig. 3a), though it is not as pronounced as the observations. The timings of the seasonal minima and maxima have been correctly simulated. The standard deviation of the daily mean N10 is also underestimated on average, where the control run for KGC has a mean standard deviation of 123 cm^{-3} compared to 342 cm^{-3} in the observations. The small variance in the model compared to the observations can also be inferred by the range of the 25th–75th percentiles.

For Macquarie Island, the control run underestimates the observations by 69 % throughout the timeseries, with summer being the most underestimated (71 %) and spring the least (64 %). The model's seasonal cycle is flat compared to the observations, indicating both missing sources of aerosol and missing seasonal processes. The control run does not capture the seasonal minima, which in the observations is shown in May after a steep decline through autumn, whilst for the model is shown in June (Fig. 3b). Note that there are limited observations (only two seasonal cycles) and that there is greater observed variability (as shown by the shading) during winter. The model again shows little variance in the winter periods, with larger variance in the summer. On average the standard deviation is observed to be 198 cm^{-3} for Macquarie Island and simulated to be 68 cm^{-3}.

Syowa, the most southerly station, shows the largest bias in aerosol concentrations from the model, with an overall underestimation of 78 %, which is largest in winter and autumn (both 81 %), and smallest in summer (74 %). Syowa has a minimum in June that is not captured by the model, which simulates the minima in August, although is generally low from May–August. The summertime maxima at Syowa is shown in the observations to occur in February, whilst is simulated in the control in December (Fig. 3c). This may be due in part to the model's treatment of sea ice and its influence on aerosol formation. On average the standard deviation of N10 for Syowa is simulated to be 66 cm^{-3} compared to the observed 427 cm^{-3}. The significant underestimation of N10 and the flat seasonal cycle at Syowa points to a considerable underestimation of small-sized aerosol in the Antarctic region, likely a missing source, such as new particles formed from biogenic precursors.

Figure 3d–g shows the seasonally and latitudinally grouped N10 medians for all the voyages. The control run (light blue) underestimates N10 in all seasons and latitudes. It also has considerably less variability (as indicated by the 25th–75th percentile range), although there is a very small sample size in some instances (shown in x-axis labels). The largest underestimation occurs in DJF for all regions: 74 %, 72 %, 74 % and 71 % from north to south. DJF has the most observations of all seasons.

Impact of sensitivity testing on N10

We now consider the experimental simulations. At KCG, switching on BL NPF (light red) has a very strong impact throughout the year, with the N10 concentrations going from an annual underestimation of 53 % to an over estimation of 290 %. For the voyage-based observations north of 45° S (Fig. 3d), we can also see a large increase in N10 across all seasons compared to the control, with the largest being in spring, though there are very few observations. For DJF, the BL NPF simulation now overestimates the northern voyage observations by 33 %. For the same season at KCG the simulation over predicted by 266 %. This large increase in small-sized aerosol may be a result of several factors, including the relative simplicity of the GLOMAP-mode BL NPF scheme (a binary scheme outlined in Sect. 2.2.1), the influence of terrestrial airmasses (which contain emissions of VOCs that mediate the BL NPF, despite our efforts to filter these influences out) or aerosol pre-cursors. A more complex NPF scheme, such as those discussed in the Introduction may yield more realistic results, while greater investigation into the observed and modelled aerosol and aerosol precursors is called for in the region.

For Macquarie Island, the inclusion of BL NPF increases the N10 concentrations marginally (underestimated by 61 % compared to control of 69 %). Macquarie Island is a small island in a region of the SO that has relatively low DMS concentrations (according to Lana et al., 2011), and therefore few local sulfuric acid sources. This, and a lack of simulated VOCs to mediate NPF likely explains the small response found when BL NPF is turned on. Similar marginal results are found in the mid-latitude voyage data (Fig. 3e).

For Syowa, turning on BL NPF has little impact. This result is unsurprising given the NPF mechanism being employed in the model, which as discussed earlier, is an organically-mediated mechanism, relying on prescribed monoterpenes, which are at their largest over terrestrial regions (excluding Antarctica). Recent literature has shown that VOCs, such as isoprene, are important in the pristine marine environments of the Southern Ocean (Ferracci et al., 2024), especially in the marginal ice zones (MIZ) where biological activity is high. These emissions are not currently considered in ACCESS. Additionally, the biological activity associated with sea ice is not explicitly included in the DMS climatologies, suggesting a potential missing source of sulfur.

Turning on PMO (yellow), which adds an additional source of aerosol into the Aitken mode, results in little change to the model performance in terms of N10. A small reduction in aerosol number across all stations and most voyage observations compared to the control run is found, moving further away from the observed N10 values. The addition of PMO aerosol may increase the rate at which aerosol are coagulating and growing, reducing the overall number of smaller-sized aerosol, and resulting in fewer overall, but larger-sized aerosol. This is found across all regions and seasons.

The original Kettle et al. (1999) DMS climatology in the Control* simulations shows larger N10 values in the summer months for most regions whilst having minimal impacts at

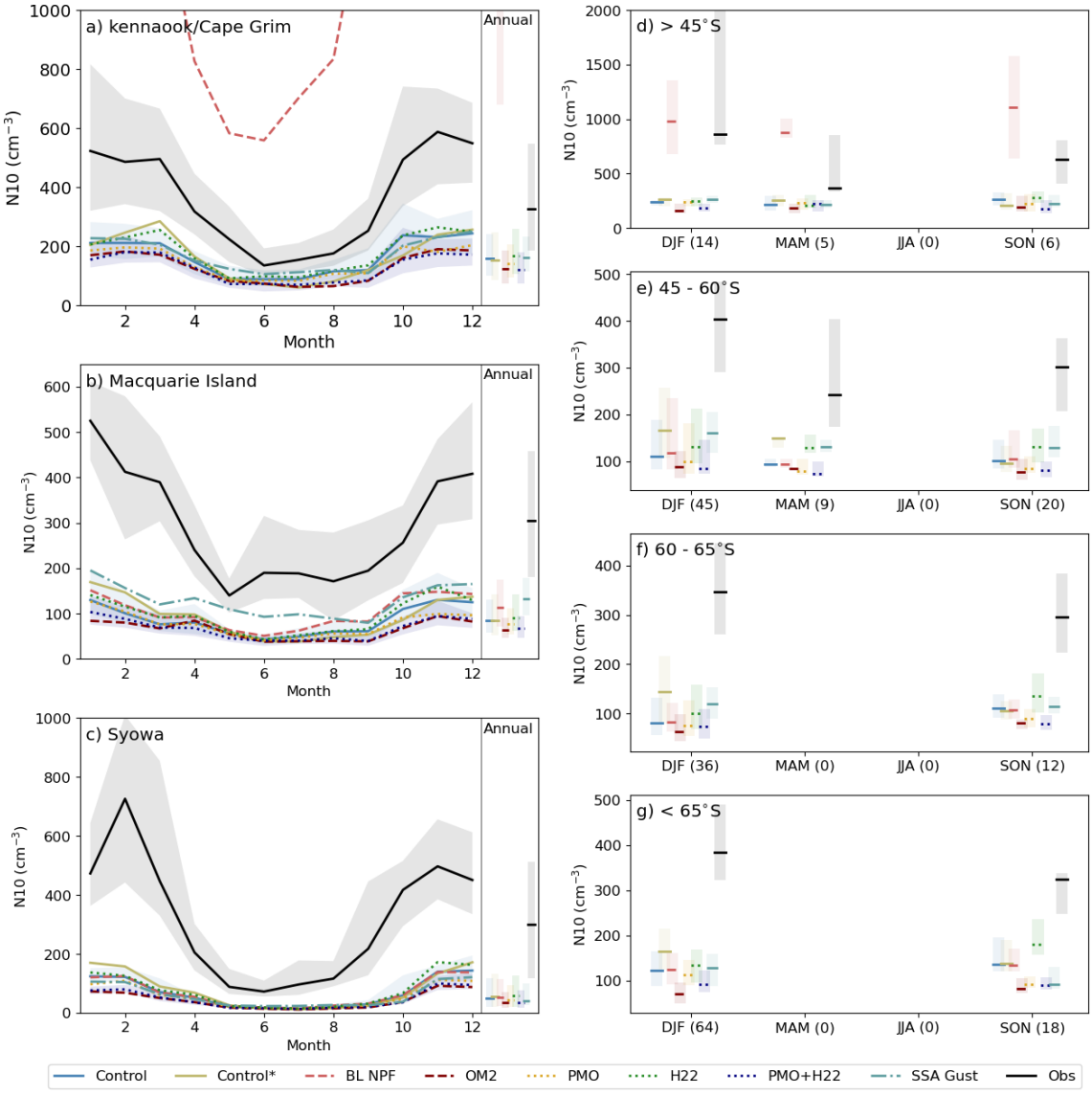

Figure 3. The monthly and annual median concentrations of daily mean N10 at **(a)** Kennaook/Cape Grim (KCG), **(b)** Macquarie Island and **(c)** Syowa and the seasonal medians for voyage data by latitude **(d)** north of 45° S, **(e)** 45–60° S, **(f)** 60–65° S and **(g)** south of 65° S. For the annual station data in **(a)**, **(b)** and **(c)** and the seasonal data in **(d)**, **(e)**, **(f)**, and **(g)** the 25th and 75th percentiles of the daily mean N10 are shown by the shaded range. For the monthly data in **(a)**, **(b)** and **(c)** the 25th–75th percentiles are just shown for the observations, control run and the experimental run PMO + H22. The observations are shown in black, while each of the model simulations are shown in colour including the control (blue), BL NPF (light red), H22 DMS (green), OM2 DMS (dark red), PMO (yellow), PMO + H22 (navy) and SSA Gust (teal). In **(a)** the BL NPF simulation at KCG shows N10 values that exceed 1500 cm m^{-3} in the warmer seasons which we believe to be unrealistic, hence we have limited the y-axis for readability. The number of observations making up the voyage values are shown in the x-axis labels in parentheses.

other times. This is especially the case for high latitude regions where the summertime DMS concentrations are very large compared to the more recent climatologies. The OM2 climatology (maroon) reduces the aerosol concentration for all sites and voyage points compared to the control. This suggests that the simple parameterisation used is not suitable for the Southern Ocean despite being a daily, time-varying climatology. Correlation values between the observations and simulations do not significantly improve between the control and OM2 simulations. The H22 DMS climatology (green) increases N10 concentration for all stations and latitudes largely in the warmer months and shoulder seasons, reflecting a slight improvement compared to the control run.

Increasing the SSA flux (teal) by using the wind gust instead of the mean wind speed again has only marginal results for the N10 concentrations, with the largest increases seen at

Macquarie Island and the mid-latitude voyage band. At Macquarie Island the annual bias goes from 69 % underestimated to 55 %, while a decrease in the N10 bias by 4 % is found at KCG and no change is found at Syowa. In the high latitude voyage data the SSA flux changes reduce the model's skill in producing N10 aerosol by approximately 17 % in SON, with little change in DJF.

Finally, we present a PMO simulation combined with the H22 DMS climatology, with the flux scaling reduced to 1.0 (from 1.7 in the control) in navy. The combination of a scaled back sulfur source and an additional source of Aitken-sized aerosol to act as surfaces for condensation has resulted in fewer N10 aerosol across all stations (an annual increase in bias of between 5 %–11 %). A similar result is found for all voyage data. This has a number of implications, for example: that the source of biogenic precursor gases may be too low across all regions; that the SSA or PMO sources should include some aerosol at smaller sizes; or that nucleation mechanisms are incorrect. A detailed study with a comprehensives suite of size and compositionally resolved observations in combination with the simulated budget terms for the aerosol (e.g. mass transfer across modes) is required to disentangle these processes.

3.2 CCN

We now consider the larger-sized aerosol range, examining observed CCN at 0.5 % supersaturation (following Humphries et al., 2023), which we compare to CCN40 in the model. We recognise that the assumptions made to compare these two fields are imperfect. Until observed size distributions are available, from which we can apply the same cut-off, our method is the best available.

For baseline KCG observations, as shown in Fig. 4a, the control run overestimates the observations by 20 %. The control run simulates the monthly minima in July, compared to August in the observations and has flatter wintertime dip in CCN concentrations. It captures the January maxima well. The annual standard deviation is 99 cm^{-3} compared to the observed 69 cm^{-3}.

For Macquarie Island, the model performs far worse than KCG, with an overall underestimation of 58 % and a standard deviation of only 29 cm^{-3} compared to 100 cm^{-3}. The model correctly simulates the summer time maxima in January, but struggles to get the observed minima correct (October in observations compared to May). In the observations, Humphries et al. (2023) show a significant wintertime peak in CCN concentrations (Fig. 4b). The authors speculated that this could be due to increased sea spray aerosol associated with higher winds during the winter. However, they noted that a large part of the second winter season was missing so the possibility of this peak being due to a few outlier events cannot be ruled out. Given the limited availability of wintertime data we cannot say if the frequency of large, individual events is common or not for this time of year. The control run shows a very small wintertime peak for the same period, but of much smaller magnitude to what was observed, which could indeed be driven by sea spray or long range transport of aerosol.

For the voyage data, Fig. 4d–g, the control run shows a general underestimation of CCN compared to the observations in all seasons and regions with a robust sample size. The results for the summer months in the northern-most latitudes have the best accuracy, being 19 % underestimated, although there is a small sample size for these statistics. For the remaining regions, all seasons are more strongly underestimated, with summer generally the strongest (58 %, 63 % and 69 % for the mid-latitudes, sub-polar and polar regions). Autumn in the mid-latitudes is approximately 43 % underestimated, with the remaining seasons and regions having too few data points for robust statistics.

Impact of sensitivity testing on CCN

For the experimental simulations, at KCG, the BL NPF simulation (light red) results in a large increase in CCN in the summer (peak in February) and spring (peak in October), with little change in the early winter months, indicating a strong signal likely due to biogenic activity. This strong signal is not as pronounced as that of the N10. For Macquarie Island, turning on BL NPF has only a small effect on these larger-sized particles, underestimating observed CCN concentrations by 54 % (compared to 59 % in the control). Similarly, for Syowa, despite no observations to compare with, we can see that turning on BL NPF does not greatly impact the CCN concentrations compared to the control simulation. For the voyage data, the largest effect of the BL NPF is found in the northernmost latitudes.

Turning on PMO has a greater impact on CCN, resulting in more CCN40-sized particles across all stations and voyage data with a robust sample size. The PMO simulation makes a strong contribution towards improving the Macquarie Island CCN concentrations from 59 % underestimated in the control to 48 %, while at KCG, it increases the overestimation by 3 %. For the voyage data, the PMO reduces the overall bias from 17 % underestimated to 2 % overestimated in the northern region, from 49 % to 33 % in the mid-latitudes region, from 64 % to 47 % in the sub-polar region and from 71 % to 60 % in the polar region.

The three changes to the DMS climatology have a much reduced impact on the CCN compared to the previous perturbations. For the Control* simulations, the annual CCN concentrations are similar to the control, with some seasonal variation. For the OM2 DMS simulation, across all stations and voyages we see a general reduction in CCN throughout the year, again indicating that this representation of DMS is not appropriate for use. For the H22 DMS, the CCN concentrations are generally similar to the control throughout the year in terms of seasonal cycle and magnitude. In spring we see marginally increased CCN in the station and voyage data.

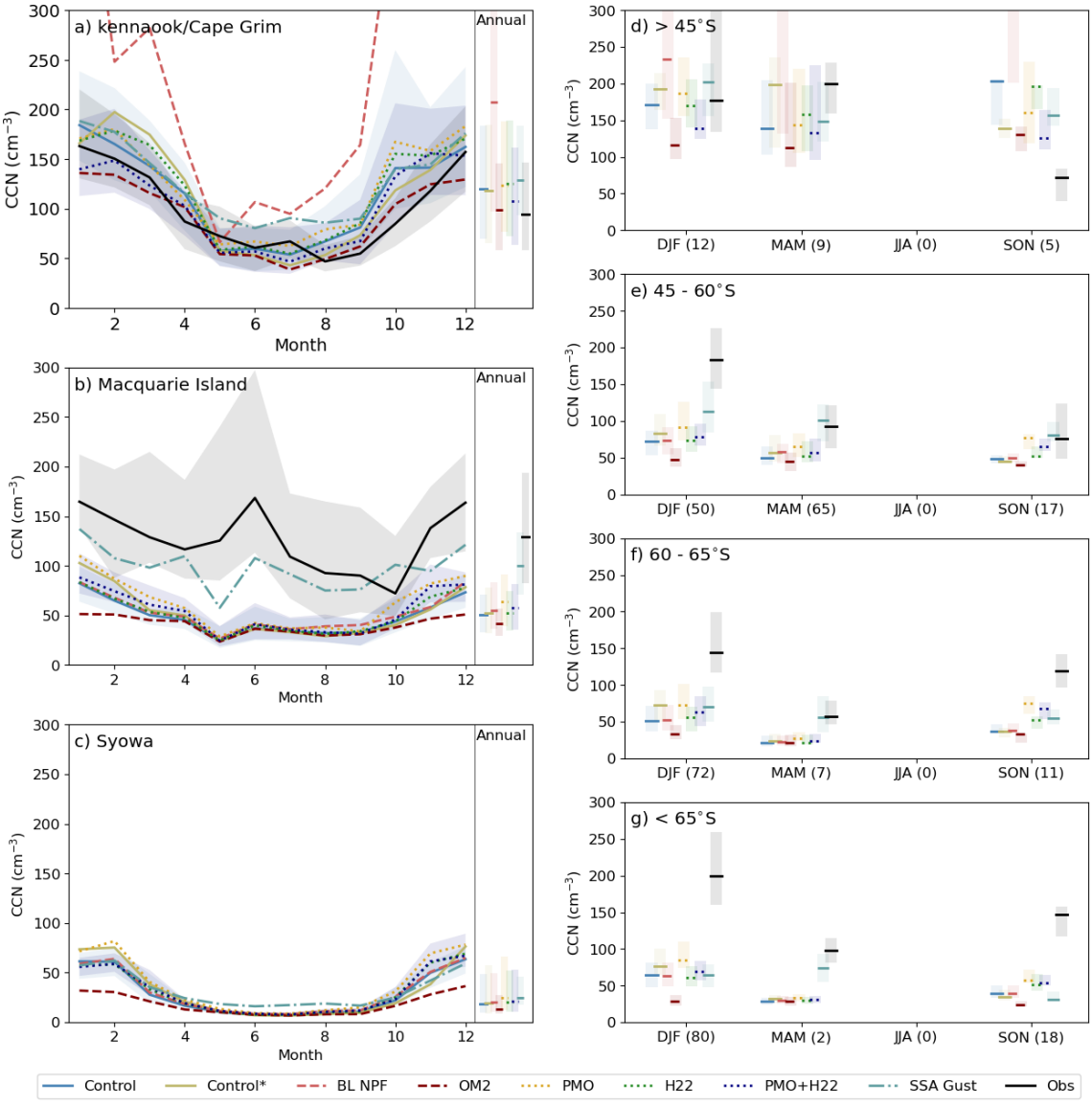

Figure 4. The monthly and annual median concentrations of CCN40 at **(a)** Kennaook/Cape Grim (KCG), **(b)** Macquarie Island and **(c)** Syowa and the seasonal medians for voyage data by latitude **(d)** north of 45° S, **(e)** 45–60° S, **(f)** 60–65° S and **(g)** south of 65° S. For the annual station data in **(a)**, **(b)** and **(c)** and the seasonal data in **(d)**, **(e)**, **(f)**, and **(g)** the 25th and 75th percentiles of the daily mean CCN40 are shown by the shaded range. For the monthly data in **(a)**, **(b)** and **(c)** the 25th–75th percentiles are just shown for the observations, control run and the experimental run PMO + H22. The observations are shown in black, while each of the model simulations are shown in colour including the control (blue), BL NPF (light red), H22 DMS (green), OM2 DMS (dark red), PMO (yellow), PMO + H22 (navy) and SSA Gust (teal). No CCN observations are available for Syowa. The number of observations making up the voyage values are shown in the x-axis labels in parentheses

Increasing the SSA flux led to large increases in CCN at Macquarie Island, where in the control, CCN was underestimated by 59 %, but is only 20 % below the observed in the SSA run. This increase in CCN (approximately 2×) is in line with that suggested by Regayre et al. (2020). The region of interest in Regayre et al. (2020) is south of Macquarie Island, where differences are smaller. The largest increases at Macquarie Island are found during the winter. For the other stations, increases in CCN are also found but not of the scale as that seen at Macquarie Island. KCG is overestimated by 30 %. At Syowa the annual median increased from 18 to 25 cm^{-3} (noting no observations to compare against at this location). For the voyage data, the SSA gust simulation generally improves the CCN representation, especially in the mid-latitude and sub-polar regions summer and autumn Fig. 4e–f.

In the PMO + H22 simulation, an improvement in CCN compared to the control simulation is found for all stations and voyages. It provides a smaller increase in CCN compared to the PMO only simulation in most marine regions (e.g. at Macquarie Island the bias is only reduced by 3 % for PMO + H22, compared to 10 % for PMO only), and reduced the CCN overestimation at KCG to just 6 %. We suggest that these differences likely reflect the reduced scaling of the H22 DMS climatology from 1.7 to 1.0. We find that the H22 climatology (scaled by 1.7) compared to the Lana climatology in the control (also scaled by 1.7) was found to have little impact on over all CCN concentrations. By scaling the DMS emissions back to 1.0, precursor gases are reduced potentially lowering the number of aerosol available to grow, or reducing the volume of condensable vapours to grow small aerosol particles to CCN sizes. This finding demonstrates the importance of considering how different aerosol sources can impact upon the potential of others to grow to climate relevant sizes.

3.3 CCN / N10 activation ratios

We now look at the activation ratios derived from the two aerosol size ranges, shown in Fig. 5. Activation ratios, where CCN is divided by the N10 concentration, are a measure of what fraction of the aerosol population can activate to be of relevance to clouds and radiation. A larger activation ratio indicates that more N10 can serve as CCN, indicating a larger-sized population (larger Aitken and accumulation mode). Lower activation ratios can indicate a smaller-sized population (nucleation or Aitken mode). As well as giving information about the size of the aerosol population, activation ratios can provide some information about the composition (Mallet et al., 2017). Activation ratios are useful to look at when aerosol size distributions are not available.

For KCG (Fig. 5) lower observed activation ratios during the warmer months indicate the presence of secondary aerosols being formed from precursor gases into the smaller modes (Humphries et al., 2023). In the cooler months, the lack of these precursor gases results in a larger population size dominated by sea spray giving a higher activation ratio. In comparison, each of the model simulations present a relatively flat seasonal cycle of activation ratio, missing entirely the wintertime peak. The larger activation ratio in the control run compared to the observations reflects the significant underestimation of the smaller-sized N10 particles, compared to the CCN which was better captured, although also underestimated. For Macquarie Island, the activation ratio is also overestimated by the control. The control simulation does show a more well-defined seasonal cycle and is within the range of observed variability in the second half of the year. The largest (wintertime) ratios in the control and observations indicate a change of influence from secondary aerosol sources to primary sources such as sea spray. During winter months at Macquarie Island the model does not reproduce the wintertime peak in CCN, compared to the observed, the activation ratio seasonal shape remains somewhat consistent with the observed. Finally, for the voyage data with a robust sample size (primarily summertime), the activation ratios for the control run compared to the observations is in most cases overestimated, except for in the high latitudes where it is underestimated.

Impact of sensitivity testing on the activation ratio

For the experimental simulations, for both the voyage data and station data broadly, the PMO (yellow), PMO + H22 (green) and SSA gust (teal) simulations have acted to increase the CCN closer to that of what is observed for most regions except that of KCG and the northern most voyage data, while having only a small impact on the N10 population. This is reflected in the activation ratios, which have in general increased above that of the control simulation, and moved further away from the observed. This highlights the model's inability to correctly capture the aerosol size distribution. The BL NPF simulation in most cases, particularly for the northern regions, reduces the activation ratio, demonstrating its large production of small-sized aerosol, which we suggest is unrealistic.

Our analysis has shown that the ACCESS-AM2 model, with GLOMAP-mode, in general does a poor job of representing aerosol populations in the Southern Ocean, with the only exception being KCG CCN, although that is still overestimated. As stated above, despite improvements to the CCN (although less so for the N10) shown for some of the experiments (e.g. PMO, PMO + H22 and SSA gust), we see a worsening of the activation ratios, suggesting that the aerosol scheme is not reflecting the reality of the Southern Ocean aerosol and the microphysical processes that govern it. A better method to diagnose these biases would be with a comparison to size distribution data, though at this time observed size distributions are only available for a few individual ship campaigns, and not for the stations of interest during this time period. Large-scale analysis of modelled aerosol size distribution compared to observations is planned. There is also work underway exploring individual campaigns.

4 Impacts on radiative forcing

A number of the experiments presented in this work have made a small but generally positive impact on the CCN (less so for the N10) for the marine and Antarctic regions studied. Before we can recommend their adoption for future releases of the model, we must consider their global impacts. In this sense, we are most interested in the impact of CCN, which are of a climatically relevant size, on the radiative balance of the Earth. As discussed in the introduction, the Southern Ocean has a persistent radiative bias, allowing too much shortwave radiation to reach the surface during austral summer, in part as a result on incorrect partitioning of cloud

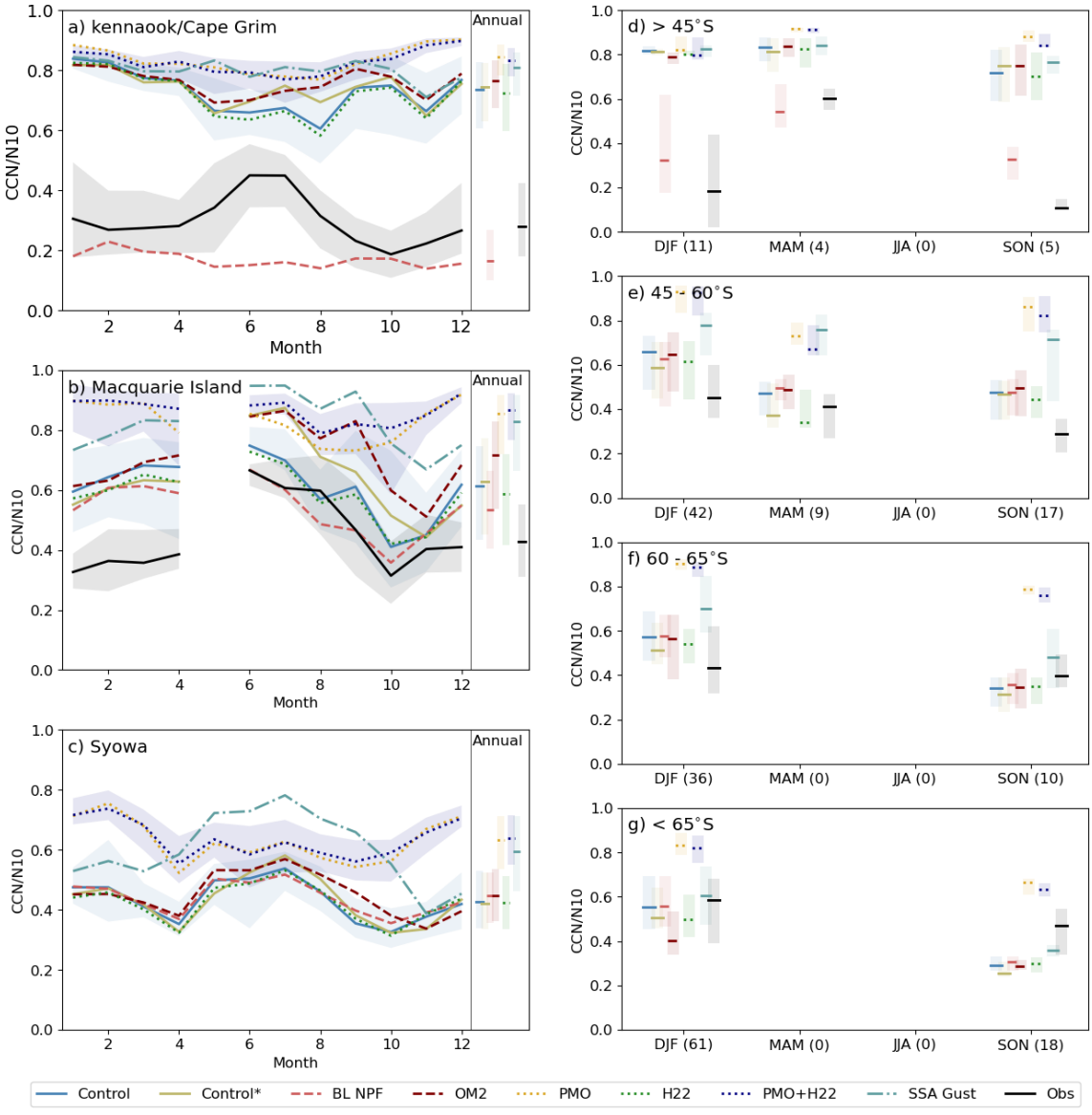

Figure 5. The monthly and annual median activation ratios (CCN40/N10) for at **(a)** Kennaook/Cape Grim, **(b)** Macquarie Island and **(c)** Syowa and the seasonal medians for voyage data by latitude **(d)** north of 45° S, **(e)** 45–60° S, **(f)** 60–65° S and **(g)** south of 65° S. For the annual station data in **(a)**, **(b)** and **(c)** and the seasonal data in **(d)**, **(e)**, **(f)**, and **(g)** the 25th and 75th percentiles of the activation ratios are shown by the shaded range. For the monthly data in **(a)**, **(b)** and **(c)** the 25th–75th percentiles are just shown for the observations, control run and the experimental run PMO + H22. The observations are shown in black, while each of the model simulations are shown in colour including the control (blue), BL NPF (light red), H22 DMS (green), OM2 DMS (dark red), PMO (yellow), PMO + H22 (navy) and SSA Gust (teal). No CCN observations are available for Syowa and hence no observed ratio. There are no concurrent days of N10 and CCN at Macquarie Island for the month of May.

phase. Previous work has explored this radiation bias in the version of the ACCESS-AM2 model evaluated here. Fiddes et al. (2022) showed that the liquid water path in the model was significantly underestimated, while the ice water path was overestimated. Fiddes et al. (2024) further suggested, using machine learning, that improvements in the model's liquid water path would have the most impact on reducing the radiative bias. Here we explore if the improvements to CCN have resulted in changes to the radiative bias, via the liquid water path.

Figure 6 shows the annual mean shortwave upwelling top of atmosphere radiation (RSUT) bias (panel a), and the changes from the control simulation for each of the experiments (panels b–h). The contour lines represent the threshold of positive to negative observed biases (as seen in panel a). Table 2 shows the change in bias from the observed for the

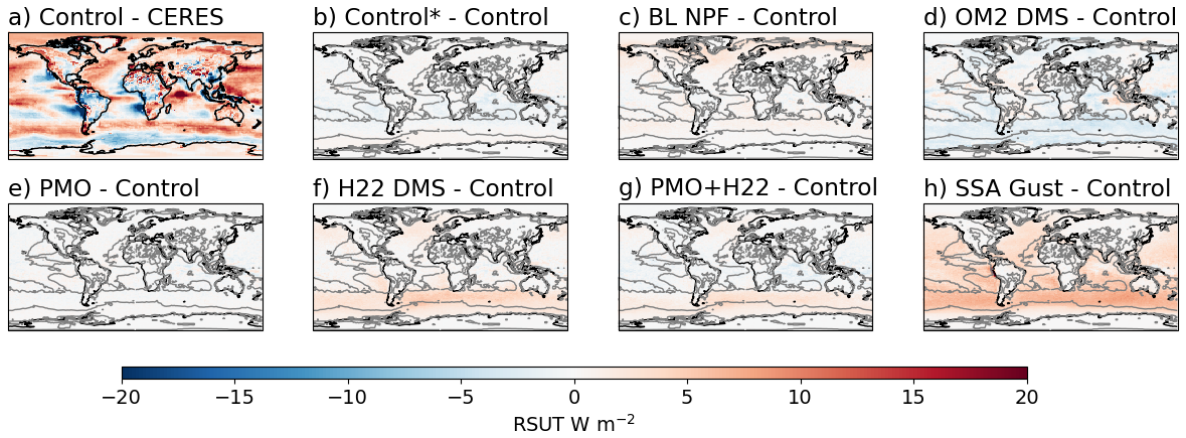

Figure 6. The annual mean radiative changes for the top of atmosphere shortwave upwelling radiation (RSUT) in $\mathrm{W\,m^{-2}}$ for **(a)** the control minus the CERES satellite, and for the experimental simulations the difference from the control for: **(b)** Control*, **(c)** BL NPF, **(d)** OM2 DMS, **(e)** PMO, **(f)** H22 DMS, **(g)** PMO + H22 and **(h)** SSA gust. For plots **(b)–(h)** the zero contour line of plot **(a)** is shown to indicate where the observational bias changes sign.

annual mean and summer time over a number of regions. Note that the regions defined in the table are not the same as those defined by Humphries et al. (2023) and used in the sections above, but match those defined in Fiddes et al. (2022) in relation to the radiative bias.

The three simulations that are considered to be the "best" in terms of improving CCN are PMO, PMO + H22 and the SSA gust simulations. Here we can see that the PMO simulation Fig. 6e has little impact on the radiative bias annually, while the combined PMO + H22 (Fig. 6g) simulation has a positive change over the Southern Ocean and a weakly negative change elsewhere. The annual polar region radiation bias is reduced from -3.43 to $-2.18\,\mathrm{W\,m^{-2}}$, while the global mean only increases by $0.2\,\mathrm{W\,m^{-2}}$. The SSA gust simulation, despite dramatically reducing the polar region bias to $-0.85\,\mathrm{W\,m^{-2}}$, shows an overall increase in the amount of reflected shortwave radiation mostly in regions outside of the Antarctic region (Fig. 6h), almost doubling the global radiative bias from 2.40 to $4.65\,\mathrm{W\,m^{-2}}$.

Figure 7 shows the liquid water path for the Control simulation and the subsequent differences from this for the experimental simulations. The changes in the annual mean shortwave radiative bias are clearly closely linked to the changes found in liquid water path, with the strongest increases over the northern parts of Southern Ocean for the SSA and H22 simulations of approximately 7.3 % and 4.5 % respectively. Increased liquid water results in clouds that are more optically thick, reflecting more radiation back out to space. Similar responses were found for the liquid cloud fraction (an overall increase, though weaker in relative terms), while insignificant positive changes were found for the ice water path (not shown).

If we consider the seasonal breakdown of the PMO + H22 simulation only (Fig. 8) we can see a clear improvement of the summertime polar Southern Ocean negative radiative bias, going from -17.78 to $-14.72\,\mathrm{W\,m^{-2}}$, with a degradation of the positive bias in the northern region of the Southern Ocean (2.37 to $5.08\,\mathrm{W\,m^{-2}}$). Autumn (MAM) and winter (JJA) season see little to no change in the top of atmosphere radiation, while we can see a positive change in spring (SON) over the northern part of the Southern Ocean.

5 Discussion

The impact of the changes in aerosol on the radiation budget raises important discussion points. Firstly, the small increase in outgoing shortwave radiation annually as a result of the H22 DMS climatology, particularly over the Southern Ocean, indicates that even a small improvement in the representation of biogenic aerosol sources can have a meaningful impact on the global radiation budget. Combining H22 with PMO, another biologically derived aerosol source, limits the increase in SW top of atmosphere radiation even further to the region of largest bias, reinforcing this idea. It also demonstrates the internal complexity of the aerosol population and the need to consider how each component influences the size and composition of the entire burden, rather than as individual (compositional) populations.

The inclusion of PMO and the H22 climatology only marginally improved the N10 and CCN concentrations, pointing towards opportunity for future work. For DMS, in the ACCESS model, a mask is applied over sea ice zones, limiting the flux of DMS in accordance with the fraction of ocean covered by sea ice. Research has shown that coastal Antarctica and sea ice regions are very biologically active and a large potential source of DMS (Trevena and Jones, 2012; Damm et al., 2016; Webb et al., 2019). None of the DMS climatologies incorporate DMS from sea ice (Lannuzel et al., 2024) which can be a dominant source in ice-covered regions (Hayashida et al., 2020). The masking of DMS by sea

Table 2. Mean outgoing top of atmosphere shortwave radiation bias (from the CERES satellite) for the annual and DJF periods, over four regions: global, Southern Ocean (43–69° S), subpolar region (43–58° S) and polar regions (58–69° S), for each simulation. We have highlighted in bold the best performing (according to the mean bias) simulation for each region/season.

	Annual				DJF			
	Glob	SO (43–69° S)	SP (43–58S)	P (58–69° S)	Glob	SO (43–69° S)	SP (43–58° S)	P (58–69° S)
Control	2.4	1.63	5.43	−3.43	0.18	−6.26	2.37	−17.78
Control*	2.32	1.87	5.49	−2.95	0.24	−5.03	3.07	−15.84
BL NPF	2.89	1.94	5.87	−3.3	0.31	−5.76	3.01	−17.45
OM2	**1.85**	**−0.09**	**3.64**	−5.06	−0.98	−10.93	−2.79	−21.78
PMO	2.37	1.7	5.44	−3.28	**−0.03**	−6.54	**1.76**	−17.62
H22	3.19	4.19	8.58	−1.65	1.33	**−1.07**	7.93	−13.06
PMO + H22	2.6	3.28	7.38	−2.18	0.4	−3.41	5.08	−14.72
SSA Gust	4.65	6.23	11.54	**−0.85**	2.69	1.12	11.18	**−12.28**

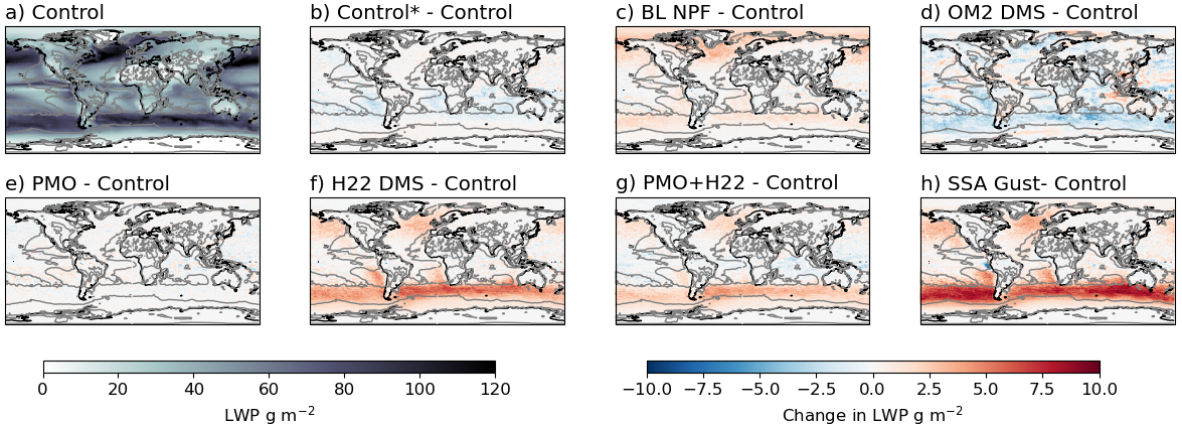

Figure 7. The annual mean liquid water path (g m^{-2}) for the Control run **(a)** and the annual mean difference in liquid water path between the experimental simulation and the Control run for: **(b)** Control*, **(c)** BL NPF, **(d)** OM2 DMS, **(e)** PMO, **(f)** H22 DMS, **(g)** PMO + H22 and **(h)** SSA gust. For plots **(b)–(h)** the zero contour line of Fig. 6a) is shown to indicate where the observational radiative bias changes sign.

ice may inhibit the potential of biological activity to influence the atmospheric composition. Representing this source of sulfate aerosol in the model may lead to a further increase of N10 and CCN in this region and a reduction in the shortwave bias. We can see some evidence of this impact if we look at the results of the Control* simulation, which, as shown, had extremely high summertime DMS concentrations in this region. The Control* simulation had larger N10 than the control, but a lesser impact on CCN, which resulted in only a small increase in outgoing shortwave radiation in this region. This suggests that the addition of a sea ice-derived DMS source would help to reduce the region of largest bias, though would not be enough on its own to fix the problem.

A known limitation of GLOMAP-mode is that it does not represent aerosol derived from methanesulfonic acid (MSA). MSA is another product of DMS oxidation in the atmosphere, as well as sulfuric acid. In GLOMAP-mode, MSA is produced in the gas phase, but is not then considered as a contributor to the aerosol burden. Revell et al. (2019) progressed MSA representation in the chemistry, adding aqueous-phase MSA. However this remains unconnected to the aerosol scheme to form MSA aerosol. The changes by Revell et al. (2019) are also not included in the offline-chemistry configuration used in this study. We suggest that adding the MSA derived aerosol to GLOMAP-mode may have some impact on increasing the aerosol burden of the Southern Ocean.

We find that BL NPF had little impact on the regions of the Southern Ocean and Antarctic least influenced by terrestrial airmasses of the mid-latitudes (south of 45° S). For regions where terrestrial airmasses are common (e.g. northern latitudes and KCG), turning on BL NPF strongly overestimates small-sized aerosol, which we suggest to be unrealistic. The shortcomings of the BL NPF scheme tested may be two fold, the first of which being that the parameterisation used (Metzger et al., 2010) is a simple binary scheme. Most global atmosphere models use classical nucleation theory involving binary NPF, though more complex ternary or ion nucleation parameterisations have also been developed. For the Antarctic, ion nucleation of sulfuric acid with ammonia (sourced from sea bird colonies) has been suggested to be an impor-

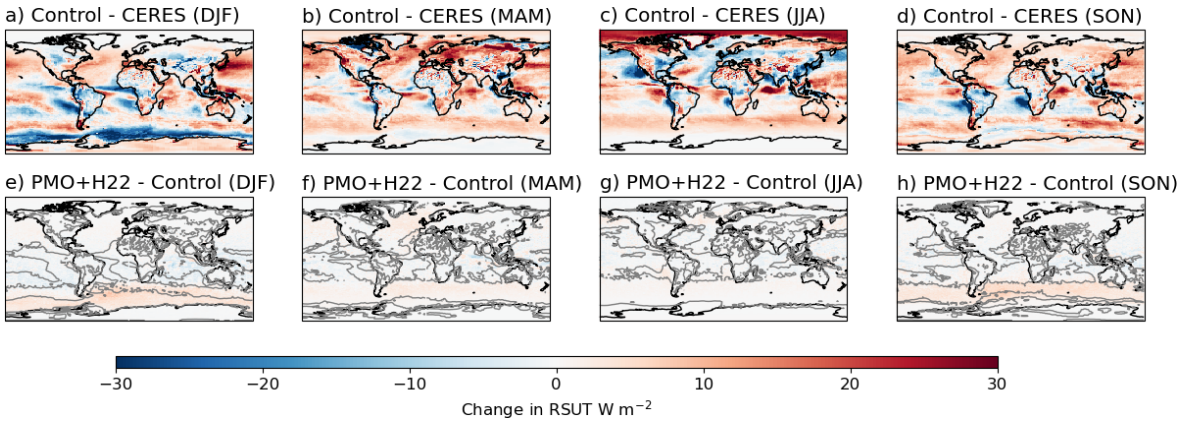

Figure 8. The radiative changes for the top of atmosphere shortwave up welling radiation (RSUT) in W m^{-2} for each season (DJF, MAM, JJA, SON from left to right) for the control minus the CERES satellite (top) and for the PMO + H22 experiment minus the conrtol (bottom). For plots **(e)**–**(h)** the zero contour line of plots **(a)**–**(d)** are shown to indicate where the observational bias changes sign.

tant pathway for nucleation (Lee et al., 2019), implying that a more complex NPF scheme could benefit this region. However, significant updates to the chemistry in ACCESS would be required to include such sources.

The second reason for the lack of response in regions dominated by marine airmasses may partly be due to a lack of marine-derived secondary organics in the model, which, in the BL NPF scheme used, mediate the reaction. For example, recent work has shown that the Southern Ocean and biologically active sea ice regions produce significant amounts of isoprene (Ferracci et al., 2024; Rodríguez-Ros et al., 2020; Brean et al., 2021; Yu and Li, 2021). This source is not included in the secondary organic climatologies for continental areas, let alone marine regions, in the version of GLOMAP used here. Secondary organics are further limited to just condensational sources within GLOMAP-mode, without the capability of forming aerosol themselves. Yu and Li (2021) have summarised that improving understanding and representation of secondary marine organics is an important step in global climate modelling (both in the free troposphere and boundary layer).

While including more detailed secondary organics in GLOMAP-mode may increase BL NPF for Southern Ocean regions, there remains a question about the reality of how much BL NPF actually occurs (not much according to Brean et al., 2021; Schmale et al., 2019). Recent campaigns near the Antarctic coastline indicate that the majority of the secondary aerosol is in fact coming from long range transport over the Antarctic continent (McCoy et al., 2021; Mace et al., 2024; Mallet et al., 2025), not particles formed in-situ. It is suggested that sulfuric acid sourced from these biologically active regions is lofted into the free troposphere where it is more likely to undergo new particle formation and growth. It is then circulated over the continent, where subsidence and katabatic outflow occur, transporting sulfate aerosol to the coastal regions at large, climatically relevant sizes. Along the coastline, a lack of precipitating clouds helps retain high CCN numbers. This long-range transport of biogenic aerosol, involving both microphysical and dynamical processes, is a crucial source of high CCN numbers in coastal Antarctic regions. To date, no study has evaluated whether an atmospheric model can replicate both the aerosol formation and long-range transport mechanisms suggested in the observations.

Finally, with respect to biologically derived aerosol, our experiments show that it is the addition of PMO that really drives the increase of CCN, by providing Aitken mode sized surfaces upon which precursor gases can condensed and grow. Currently in ACCESS the PMO is derived from a fractional assumption of the sea spray using chlorophyll-*a* as the reference for biological activity. A recent review has suggested that chlorophyll-*a* may not be a good general proxy for organics (Russell et al., 2023). Furthermore, the assumption that all PMO is released into the Aitken mode (as is currently done) may also be an oversimplification of this process (Quinn et al., 2015; Prather et al., 2013).

While the changes in radiative forcing is small as a result of PMO here, we must also consider its potential impact on cloud phase. PMO is a source of ice nucleating particle, and significant effort globally is being undertaken to link INP directly to cloud schemes, instead of using empirical temperature based parameterisations. These efforts rely on the accurate representation of aerosol composition and highlights the need for comprehensive compositional data for model development, as shown in McCluskey et al. (2023). In the next generation of ACCESS models, which should include new double moment cloud microphysics (Field et al., 2023), we hope to be able to make this direct connection from aerosol to cloud phase.

Overall, small improvements to the CCN as a result of improving biologically derived aerosol representation has helped the summer time radiative bias in the southern regions

of the Southern Ocean, albeit with some errors in spring. This does suggest that if we can better represent the biological cycle in our climate models, we may have a better chance of simulating the aerosol-climate system.

On the other hand, our experiments using SSA derived from the wind gusts show significant (albeit unphysical) improvements in CCN over the mid-latitude ranges of the Southern Ocean. A later update to the GLOMAP-mode dry deposition velocities has lead to increased coarse-mode deposition velocities that reportedly impact the sea-salt aerosol distribution (Mulcahy et al., 2020). We speculate that this update may reduce the magnitude of impact of our SSA changes on the CCN. While the improvement in CCN was intended, it also resulted in a significant degradation of the shortwave radiation bias for the region (the bias becomes more positive). While a positive change is desirable further south of Macquarie Island (where the radiative bias is negative), to the north of this region, a positive change results in a larger positive radiative bias. This is particularly concerning as this region has been highlighted as an area of large uncertainty in cloud feedbacks (Zelinka et al., 2020), and aerosol-cloud interaction is understood to be one of the most uncertain components of this. In this instance, improving the CCN in a key area of uncertainty in the Southern Ocean had detrimentally affected the radiative bias, which worsens the models bias in the global energy balance by a factor of two.

These results point to at least two possible conclusions. The first is that the model and its constituent components has been so highly tuned that the improvement of the physical representation of particular components results in a worsening of downstream systems. The second is that the biases in CCN in the model have been masking potentially even worse biases within the cloud scheme, and by improving the aerosol representation, we are revealing these errors. In reality, it is likely that these two hypotheses are inextricably linked and points to a need to consider model development as an entire system rather than individual components.

6 Conclusions

The Southern Ocean aerosol population has been shown here to be poorly simulated by a sophisticated double moment aerosol scheme, GLOMAP-mode, within the ACCESS-AM2 atmospheric model. Simulated N10 aerosol are strongly underestimated in all regions examined. Outside of continental Australian influences, larger CCN-sized aerosol numbers are also underestimated. Our attempts to increase these populations have been limited in success. To summarise, turning on BL NPF significantly increases N10 only in Australian continentally influenced regions, having little impact on either N10 or CCN in other regions. The use of a time varying, parameterised DMS climatology resulted in reductions in aerosol number, indicating that the parameterisation used is not suitable for this region. Updating the DMS climatology to the new H22 dataset made only small differences to aerosol number. Reducing the DMS flux scaling to 1.0 (from 1.7) and adding PMO increased CCN whilst also decreasing N10. Turning on PMO alone showed larger increases in CCN, possibly resulting from faster growth to larger-sized aerosol. Finally, increasing the SSA flux in line with wind gusts instead of mean wind speed strongly increased CCN in the marine regions, particularly in winter.

Our results have demonstrated issues with capturing the size and number of aerosol populations, and points towards missing aerosol sources and possibly issues within the aerosol scheme structure or microphysics. We reiterate a strong need for comprehensive aerosol observations in the Southern Ocean region to inform model development, including size and compositional information.

From our experiments, we suggest that future versions of ACCESS do consider using the H22 DMS climatology, with emissions scaled to 1.0, in combination with the PMO turned on. Switching on PMO and re-scaling DMS brings ACCESS in line with more recent versions of the UM global atmosphere configurations (Mulcahy et al., 2020), while the H22 data-set represents the newest knowledge in terms of DMS concentrations.

The impacts of these changes on the radiative balance have also been investigated. The H22 + PMO combined experiment yielded the best results as far as improving the Southern Ocean radiative bias, whilst having limited adverse effects restricted to the northern parts of the Southern Ocean in springtime. The SSA gust experiment had the largest impact, increasing the amount of shortwave radiation reflected out to space across the globe, with large, undesirable effects on beyond the Southern Ocean. This result is of particular concern given that large improvements to the CCN in this simulation has resulted in untenable increase of the radiative bias in the southern hemisphere mid-high latitudes, a key area of uncertainty for cloud feedbacks.

We draw two main conclusions from this work, corresponding to two different regions of the Southern Ocean. We suggest that better capturing the biological influence on aerosol may lead to limited improvements in the aerosol-cloud-radiative system of the Southern Ocean's sea-ice regions, where the radiative bias is at its worst. We also show that in order to reduce the uncertainty of cloud feedbacks and the energy balance in the northern parts of the Southern Ocean, improving the aerosol alone is not effective (in fact is detrimental) but may be a pre-requisite for improving aerosol-cloud interactions due to the influence of aerosol composition and size.

Code and data availability. All model data is hosted on Zenodo at https://doi.org/10.5281/zenodo.13864183 (Fiddes, 2024). Code for this project is provided on GitHub via https://github.com/sfiddes/ACCESS_aerosol_eval (last access: 17 November 2025; DOI: https://doi.org/10.5281/zenodo.17626077, Fiddes, 2025). CN and CCN data from Macquarie Island are available at https://doi.org/10.25919/g7jx-k629 (Humphries et al., 2021b). Data from Kennaook/Cape Grim are available at the World Data Centre for Aerosols at https://ebas-data.nilu.no (Keywood et al., 2023a, b). Syowa data are available at https://doi.org/10.17592/002.2023030399 (Hara, 2023). Data from MARCUS are available at https://doi.org/10.25919/ezp0-em87 (Humphries, 2020). Cold Water Trial data are available at https://doi.org/10.25919/ytsw-9610 (Humphries et al., 2022b). CAPRICORN1 data are available at https://doi.org/10.25919/5f688fcc97166 (Protat, 2020). Ice2Equator data are available at https://doi.org/10.25919/g07r-b187 (Humphries et al., 2022a). PCAN data are available at https://doi.org/10.25919/xs0b-an24 (Humphries et al., 2020b). CAPRICORN2 data are available at https://doi.org/10.25919/2h1c-t753 (Humphries et al., 2020a). CAMMPCAN data are available at https://doi.org/10.26179/5e546f452145d (Schofield and Ryan, 2021).

Author contributions. SF has performed the analysis, writing and model simulations. MW provided advice and assistance with the model simulations. RH led the collection and quality control for the ship-based aerosol observations presented here, and was involved in the collation the remainder of the observations used. MM has provided expert advise on observed aerosol characteristics and experimental setup. This study has expanded upon LL's Honours thesis (supervised by SF, MW and RH), which provided an initial concept of this study. SP and AP have provided guidance throughout this study. HH developed the OM2 DMS dataset. BM, SP, RH and RS provided the quality controlled CAMMPCAN observations, and RS additional compute resources. All authors have contributed to the revisions of this manuscript.

Competing interests. The contact author has declared that none of the authors has any competing interests.

Disclaimer. Publisher's note: Copernicus Publications remains neutral with regard to jurisdictional claims made in the text, published maps, institutional affiliations, or any other geographical representation in this paper. While Copernicus Publications makes every effort to include appropriate place names, the final responsibility lies with the authors. Views expressed in the text are those of the authors and do not necessarily reflect the views of the publisher.

Acknowledgements. We would like to thank the useful discussions with Peter May which led to the changes in the sea spray flux parameterisation. Resources and services from the National Computational Infrastructure (Project jk72, gx60, v45 and q90), supported by the Australian Government, were used. S.F. acknowledges the Australian Research Council Centre of Excellence for Climate Extremes and the Australian Community Climate Earth System Simulator National Research Infrastructure, funded by the Australian Government's National Collaborative Research Infrastructure Strategy, for their maintenance of virtual environments, code and model support. The authors would like to acknowledge the teams at NASA CERES for making the radiation data used in this work publicly available. The Authors wish to thank the CSIRO Marine National Facility (MNF) for its support in the form of sea time on RV *Investigator*, support personnel, scientific equipment and data management. All data and samples acquired on the voyage are made publicly available in accordance with MNF Policy. We would also like to thank the teams at Kennaook/Cape Grim, led by Melita Keywood, and the Korean station Syowa, led by Keiichiro Hara, for their work in producing the datasets used here. Technical and logistical support for the deployment to Macquarie Island were provided by the Australian Antarctic Division through Australian Antarctic Science Project 4292, and we thank George Brettingham-Moore, Ken Barrett, Nick Cartwright, Nick Cole (deceased), Emry Crocker, Terry Egan, John French, Eric King (deceased), Ian McRobert, Lloyd Symons, Peter de Vries and Steven Whiteside for all of their assistance. Technical and logistical support for the deployment of CAMMPCAN on the RSV Aurora Australis 2017–2018 and 2018–2019 by the Australian Antarctic Division through Australian Antarctic Science Project 4431. AIRBOX was funded by the Australian Research Council LIEF grant: LE150100048.

Financial support. This project received grant funding from the Australian Government as part of the Antarctic Science Collaboration Initiative program, under the Australian Antarctic Program Partnership, ASCI000002.

Review statement. This paper was edited by Ann Fridlind and reviewed by three anonymous referees.

References

Albrecht, B. A.: Aerosols, cloud microphysics, and fractional cloudiness, Science, 245, 1227–1230, https://doi.org/10.1126/science.245.4923.1227, 1989.

Alinejadtabrizi, T., Lang, F., Huang, Y., Ackermann, L., Keywood, M., Ayers, G., Krummel, P., Humphries, R., Williams, A. G., Siems, S. T., and Manton, M.: Wet deposition in shallow convection over the Southern Ocean, npj Climate and Atmospheric Science, 7, 1–12, https://doi.org/10.1038/S41612-024-00625-1, 2024.

Alroe, J., Cravigan, L. T., Miljevic, B., Johnson, G. R., Selleck, P., Humphries, R. S., Keywood, M. D., Chambers, S. D., Williams, A. G., and Ristovski, Z. D.: Marine productivity and synoptic meteorology drive summer-time variability in Southern Ocean aerosols, Atmos. Chem. Phys., 20, 8047–8062, https://doi.org/10.5194/acp-20-8047-2020, 2020.

Aranami, K. and Tsunogai, S.: Seasonal and regional comparison of oceanic and atmospheric dimethylsulfide in the northern North Pacific: Dilution effects on its concentration during

winter, Journal of Geophysical Research D: Atmospheres, 109, https://doi.org/10.1029/2003JD004288, 2004.

Bell, T. G., Landwehr, S., Miller, S. D., de Bruyn, W. J., Callaghan, A. H., Scanlon, B., Ward, B., Yang, M., and Saltzman, E. S.: Estimation of bubble-mediated air–sea gas exchange from concurrent DMS and CO_2 transfer velocities at intermediate–high wind speeds, Atmos. Chem. Phys., 17, 9019–9033, https://doi.org/10.5194/acp-17-9019-2017, 2017.

Bhatti, Y. A., Revell, L. E., Schuddeboom, A. J., McDonald, A. J., Archibald, A. T., Williams, J., Venugopal, A. U., Hardacre, C., and Behrens, E.: The sensitivity of Southern Ocean atmospheric dimethyl sulfide (DMS) to modeled oceanic DMS concentrations and emissions, Atmos. Chem. Phys., 23, 15181–15196, https://doi.org/10.5194/acp-23-15181-2023, 2023

Bi, D., Dix, M., Marsland, S., O'Farrell, S., Sullivan, A., Bodman, R., Law, R., Harman, I., Srbinovsky, J., Rashid, H. A., Dobrohotoff, P., Mackallah, C., Yan, H., Hirst, A., Savita, A., Dias, F. B., Woodhouse, M., Fiedler, R., and Heerdegen, A.: Configuration and spin-up of ACCESS-CM2, the new generation Australian Community Climate and Earth System Simulator Coupled Model, Journal of Southern Hemisphere Earth Systems Science, 70, 225–251, https://doi.org/10.1071/es19040, 2020.

Bock, J., Michou, M., Nabat, P., Abe, M., Mulcahy, J. P., Olivié, D. J. L., Schwinger, J., Suntharalingam, P., Tjiputra, J., van Hulten, M., Watanabe, M., Yool, A., and Séférian, R.: Evaluation of ocean dimethylsulfide concentration and emission in CMIP6 models, Biogeosciences, 18, 3823–3860, https://doi.org/10.5194/bg-18-3823-2021, 2021.

Bodas-Salcedo, A., Williams, K. D., Ringer, M. A., Beau, I., Cole, J. N. S., Dufresne, J. L., Koshiro, T., Stevens, B., Wang, Z., and Yokohata, T.: Origins of the solar radiation biases over the Southern Ocean in CFMIP2 models, Journal of Climate, 27, 41–56, https://doi.org/10.1175/JCLI-D-13-00169.1, 2014.

Bodman, R. W., Karoly, D. J., Dix, M. R., Harman, I. N., Srbinovsky, J., Dobrohotoff, P. B., and Mackallah, C.: Evaluation of CMIP6 AMIP climate simulations with the ACCESS-AM2 model, Journal of Southern Hemisphere Earth Systems Science, 70, 166–179, https://doi.org/10.1071/ES19033, 2020.

Boucher, O., Randall, D., Artaxo, P., Bretherton, C., Feingold, G., Forster, P., Kerminen, V. M., Kondo, Y., Liao, H., Lohmann, U., Rasch, P., Satheesh, S. K., Sherwood, S., Stevens, B., Zhang, X. Y., and Zhan, X. Y.: Clouds and Aerosols, in: Climate Change 2013: The Physical Science Basis. Contribution of Working Group I to the Fifth Assessment Report of the Intergovernmental Panel on Climate Change, edited by: Stocker, T., Qin, D., Plattner, G.-K., Tignor, M., Allen, S., Boschung, J., Nauels, A., Xia, Y., Bex, V., and Midgley, P., 571–657, Cambridge University Press, Cambridge, United Kingdom and New York, NY, USA, https://doi.org/10.1017/CBO9781107415324.016, 2013.

Brean, J., Dall'Osto, M., Simó, R., Shi, Z., Beddows, D. C. S., and Harrison, R. M.: Open ocean and coastal new particle formation from sulfuric acid and amines around the Antarctic Peninsula, Nature Geoscience, https://doi.org/10.1038/s41561-021-00751-y, 2021.

Burrows, S. M., McCluskey, C. S., Cornwell, G., Steinke, I., Zhang, K., Zhao, B., Zawadowicz, M., Raman, A., Kulkarni, G., China, S., Zelenyuk, A., and DeMott, P. J.: Ice-Nucleating Particles That Impact Clouds and Climate: Observational and Modeling Research Needs, Reviews of Geophysics, 60, https://doi.org/10.1029/2021RG000745, 2022.

Carslaw, K. S., Lee, L. A., Reddington, C. L., Pringle, K. J., Rap, A., Forster, P. M., Mann, G. W., Spracklen, D. V., Woodhouse, M. T., Regayre, L. A., and Pierce, J. R.: Large contribution of natural aerosols to uncertainty in indirect forcing, Nature, 503, 67–71, https://doi.org/10.1038/nature12674, 2013.

Curtius, J.: Nucleation of atmospheric aerosol particles, Comptes Rendus. Physique, Nucleation, 7, 1027–1045, https://doi.org/10.1016/j.crhy.2006.10.018, 2006.

Damm, E., Nomura, D., Martin, A., Dieckmann, G. S., and Meiners, K. M.: DMSP and DMS cycling within Antarctic sea ice during the winter–spring transition, Deep-Sea Research Part II: Topical Studies in Oceanography, 131, 150–159, https://doi.org/10.1016/j.dsr2.2015.12.015, 2016.

De Leeuw, G., Andreas, E. L., Anguelova, M. D., Fairall, C. W., Lewis, E. R., O'Dowd, C., Schulz, M., and Schwartz, S. E.: Production flux of sea spray aerosol, Reviews of Geophysics, 49, https://doi.org/10.1029/2010RG000349, 2011.

Doelling, D. R., Loeb, N. G., Keyes, D. F., Nordeen, M. L., Morstad, D., Nguyen, C., Wielicki, B. A., Young, D. F., and Sun, M.: Geostationary enhanced temporal interpolation for ceres flux products, Journal of Atmospheric and Oceanic Technology, 30, 1072–1090, https://doi.org/10.1175/JTECH-D-12-00136.1, 2013.

Doelling, D. R., Sun, M., Nguyen, L. T., Nordeen, M. L., Haney, C. O., Keyes, D. F., and Mlynczak, P. E.: Advances in geostationary-derived longwave fluxes for the CERES synoptic (SYN1deg) product, Journal of Atmospheric and Oceanic Technology, 33, 503–521, https://doi.org/10.1175/JTECH-D-15-0147.1, 2016.

Eyring, V., Bony, S., Meehl, G. A., Senior, C. A., Stevens, B., Stouffer, R. J., and Taylor, K. E.: Overview of the Coupled Model Intercomparison Project Phase 6 (CMIP6) experimental design and organization, Geosci. Model Dev., 9, 1937–1958, https://doi.org/10.5194/gmd-9-1937-2016, 2016.

Feng, L., Smith, S. J., Braun, C., Crippa, M., Gidden, M. J., Hoesly, R., Klimont, Z., van Marle, M., van den Berg, M., and van der Werf, G. R.: The generation of gridded emissions data for CMIP6, Geosci. Model Dev., 13, 461–482, https://doi.org/10.5194/gmd-13-461-2020, 2020.

Ferracci, V., Weber, J., Bolas, C. G., Robinson, A. D., Tummon, F., Rodríguez-Ros, P., Cortés-Greus, P., Baccarini, A., Jones, R. L., Galí, M., Simó, R., Schmale, J., and Harris, N. R. P.: Atmospheric isoprene measurements reveal larger-than-expected Southern Ocean emissions, Nature Communications, 15, 2571, https://doi.org/10.1038/s41467-024-46744-4, 2024.

Fiddes, S. L.: ACCESS-AM2 campaign data (1.0.0), Zenodo [data set], https://doi.org/10.5281/zenodo.13864183, 2024.

Fiddes, S.: sfiddes/ACCESS_aerosol_eval: ACCESS aerosol eval code published in ACP, Zenodo [code], https://doi.org/10.5281/zenodo.17626077, 2024b.

Fiddes, S. L., Woodhouse, M. T., Nicholls, Z., Lane, T. P., and Schofield, R.: Cloud, precipitation and radiation responses to large perturbations in global dimethyl sulfide, Atmos. Chem. Phys., 18, 10177–10198, https://doi.org/10.5194/acp-18-10177-2018, 2018.

Fiddes, S. L., Protat, A., Mallet, M. D., Alexander, S. P., and Woodhouse, M. T.: Southern Ocean cloud and shortwave radiation biases in a nudged climate model simulation: does the

model ever get it right?, Atmos. Chem. Phys., 22, 14603–14630, https://doi.org/10.5194/acp-22-14603-2022, 2022.

Fiddes, S. L., Mallet, M. D., Protat, A., Woodhouse, M. T., Alexander, S. P., and Furtado, K.: A machine learning approach for evaluating Southern Ocean cloud radiative biases in a global atmosphere model, Geosci. Model Dev., 17, 2641–2662, https://doi.org/10.5194/gmd-17-2641-2024, 2024.

Field, P. R., Hill, A., Shipway, B., Furtado, K., Wilkinson, J., Miltenberger, A., Gordon, H., Grosvenor, D. P., Stevens, R., and Van Weverberg, K.: Implementation of a double moment cloud microphysics scheme in the UK met office regional numerical weather prediction model, Quarterly Journal of the Royal Meteorological Society, https://doi.org/10.1002/qj.4414, 2023.

Forster, P., Storelvmo, T., Armour, K., Collins, W., Dufresne, J.-L., Frame, D., Lunt, D. J., Mauritsen, T., Palmer, M. D., Watanabe, M., Wild, M., and Zhang, H.: The Earth's Energy Budget, Climate Feedbacks and Climate Sensitivity, in: Climate Change 2021 – The Physical Science Basis, 923–1054, Cambridge University Press, https://doi.org/10.1017/9781009157896.009, 2023.

Fossum, K. N., Ovadnevaite, J., Ceburnis, D., Dall'Osto, M., Marullo, S., Bellacicco, M., Simó, R., Liu, D., Flynn, M., Zuend, A., and O'Dowd, C.: Summertime Primary and Secondary Contributions to Southern Ocean Cloud Condensation Nuclei, Scientific Reports, 8, 13844, https://doi.org/10.1038/s41598-018-32047-4, 2018.

Fricko, O., Havlik, P., Rogelj, J., Klimont, Z., Gusti, M., Johnson, N., Kolp, P., Strubegger, M., Valin, H., Amann, M., Ermolieva, T., Forsell, N., Herrero, M., Heyes, C., Kindermann, G., Krey, V., McCollum, D. L., Obersteiner, M., Pachauri, S., Rao, S., Schmid, E., Schoepp, W., and Riahi, K.: The marker quantification of the Shared Socioeconomic Pathway 2: A middle-of-the-road scenario for the 21st century, Global Environmental Change, 42, 251–267, https://doi.org/10.1016/j.gloenvcha.2016.06.004, 2017.

Galí, M., Levasseur, M., Devred, E., Simó, R., and Babin, M.: Sea-surface dimethylsulfide (DMS) concentration from satellite data at global and regional scales, Biogeosciences, 15, 3497–3519, https://doi.org/10.5194/bg-15-3497-2018, 2018.

Gantt, B., Meskhidze, N., Facchini, M. C., Rinaldi, M., Ceburnis, D., and O'Dowd, C. D.: Wind speed dependent size-resolved parameterization for the organic mass fraction of sea spray aerosol, Atmos. Chem. Phys., 11, 8777–8790, https://doi.org/10.5194/acp-11-8777-2011, 2011.

Gantt, B., Johnson, M. S., Meskhidze, N., Sciare, J., Ovadnevaite, J., Ceburnis, D., and O'Dowd, C. D.: Model evaluation of marine primary organic aerosol emission schemes, Atmos. Chem. Phys., 12, 8553–8566, https://doi.org/10.5194/acp-12-8553-2012, 2012.

Gidden, M. J., Riahi, K., Smith, S. J., Fujimori, S., Luderer, G., Kriegler, E., van Vuuren, D. P., van den Berg, M., Feng, L., Klein, D., Calvin, K., Doelman, J. C., Frank, S., Fricko, O., Harmsen, M., Hasegawa, T., Havlik, P., Hilaire, J., Hoesly, R., Horing, J., Popp, A., Stehfest, E., and Takahashi, K.: Global emissions pathways under different socioeconomic scenarios for use in CMIP6: a dataset of harmonized emissions trajectories through the end of the century, Geosci. Model Dev., 12, 1443–1475, https://doi.org/10.5194/gmd-12-1443-2019, 2019.

Gong, S. L.: A parameterization of sea-salt aerosol source function for sub- and super-micron particles, Global Biogeochemical Cycles, 17, https://doi.org/10.1029/2003GB002079, 2003.

Gordon, H., Sengupta, K., Rap, A., Duplissy, J., Frege, C., Williamson, C., Heinritzi, M., Simon, M., Yan, C., Almeida, J., Tröstl, J., Nieminen, T., Ortega, I. K., Wagner, R., Dunne, E. M., Adamov, A., Amorim, A., Bernhammer, A.-K., Bianchi, F., Breitenlechner, M., Brilke, S., Chen, X., Craven, J. S., Dias, A., Ehrhart, S., Fischer, L., Flagan, R. C., Franchin, A., Fuchs, C., Guida, R., Hakala, J., Hoyle, C. R., Jokinen, T., Junninen, H., Kangasluoma, J., Kim, J., Kirkby, J., Krapf, M., Kürten, A., Laaksonen, A., Lehtipalo, K., Makhmutov, V., Mathot, S., Molteni, U., Monks, S. A., Onnela, A., Peräkylä, O., Piel, F., Petäjä, T., Praplan, A. P., Pringle, K. J., Richards, N. A. D., Rissanen, M. P., Rondo, L., Sarnela, N., Schobesberger, S., Scott, C. E., Seinfeld, J. H., Sharma, S., Sipilä, M., Steiner, G., Stozhkov, Y., Stratmann, F., Tomé, A., Virtanen, A., Vogel, A. L., Wagner, A. C., Wagner, P. E., Weingartner, E., Wimmer, D., Winkler, P. M., Ye, P., Zhang, X., Hansel, A., Dommen, J., Donahue, N. M., Worsnop, D. R., Baltensperger, U., Kulmala, M., Curtius, J., and Carslaw, K. S.: Reduced anthropogenic aerosol radiative forcing caused by biogenic new particle formation, Proceedings of the National Academy of Sciences, 113, 12053–12058, https://doi.org/10.1073/pnas.1602360113, 2016.

Gras, J. L. and Keywood, M.: Cloud condensation nuclei over the Southern Ocean: wind dependence and seasonal cycles, Atmos. Chem. Phys., 17, 4419–4432, https://doi.org/10.5194/acp-17-4419-2017, 2017.

Grythe, H., Ström, J., Krejci, R., Quinn, P., and Stohl, A.: A review of sea-spray aerosol source functions using a large global set of sea salt aerosol concentration measurements, Atmos. Chem. Phys., 14, 1277–1297, https://doi.org/10.5194/acp-14-1277-2014, 2014.

Hara, K.: Antarctic aerosol CN, National Institute of Polar Research [data set], https://doi.org/10.17592/002.2023030399, 2023.

Hara, K., Osada, K., Nishita-Hara, C., and Yamanouchi, T.: Seasonal variations and vertical features of aerosol particles in the Antarctic troposphere, Atmos. Chem. Phys., 11, 5471–5484, https://doi.org/10.5194/acp-11-5471-2011, 2011.

Hara, K., Nishita-Hara, C., Osada, K., Yabuki, M., and Yamanouchi, T.: Characterization of aerosol number size distributions and their effect on cloud properties at Syowa Station, Antarctica, Atmos. Chem. Phys., 21, 12155–12172, https://doi.org/10.5194/acp-21-12155-2021, 2021.

Hartery, S., Toohey, D., Revell, L., Sellegri, K., Kuma, P., Harvey, M., and McDonald, A. J.: Constraining the Surface Flux of Sea Spray Particles From the Southern Ocean, Journal of Geophysical Research: Atmospheres, 125, 1–19, https://doi.org/10.1029/2019JD032026, 2020.

Hayashida, H., Carnat, G., Galí, M., Monahan, A. H., Mortenson, E., Sou, T., and Steiner, N. S.: Spatiotemporal Variability in Modeled Bottom Ice and Sea Surface Dimethylsulfide Concentrations and Fluxes in the Arctic During 1979–2015, Global Biogeochemical Cycles, 34, https://doi.org/10.1029/2019GB006456, 2020.

Hayashida, H., Jin, M., Steiner, N. S., Swart, N. C., Watanabe, E., Fiedler, R., Hogg, A. McC., Kiss, A. E., Matear, R. J., and Strutton, P. G.: Ice Algae Model Intercomparison

Project phase 2 (IAMIP2), Geosci. Model Dev., 14, 6847–6861, https://doi.org/10.5194/gmd-14-6847-2021, 2021.

Hersbach, H., Bell, B., Berrisford, P., Hirahara, S., Horányi, A., Muñoz-Sabater, J., Nicolas, J., Peubey, C., Radu, R., Schepers, D., Simmons, A., Soci, C., Abdalla, S., Abellan, X., Balsamo, G., Bechtold, P., Biavati, G., Bidlot, J., Bonavita, M., Chiara, G., Dahlgren, P., Dee, D., Diamantakis, M., Dragani, R., Flemming, J., Forbes, R., Fuentes, M., Geer, A., Haimberger, L., Healy, S., Hogan, R. J., Hólm, E., Janisková, M., Keeley, S., Laloyaux, P., Lopez, P., Lupu, C., Radnoti, G., Rosnay, P., Rozum, I., Vamborg, F., Villaume, S., and Thépaut, J.: The ERA5 global reanalysis, Quarterly Journal of the Royal Meteorological Society, 146, 1999–2049, https://doi.org/10.1002/qj.3803, 2020.

Horsley, J. A., Broome, R. A., Johnston, F. H., Cope, M., and Morgan, G. G.: Health burden associated with fire smoke in Sydney, 2001–2013, Medical Journal of Australia, 208, 309–310, https://doi.org/10.5694/mja18.00032, 2018.

Hoyer, S. and Hamman, J. J.: xarray: N-D labeled Arrays and Datasets in Python, Journal of Open Research Software, 5, https://doi.org/10.5334/jors.148, 2017.

Hulswar, S., Simó, R., Galí, M., Bell, T. G., Lana, A., Inamdar, S., Halloran, P. R., Manville, G., and Mahajan, A. S.: Third revision of the global surface seawater dimethyl sulfide climatology (DMS-Rev3), Earth Syst. Sci. Data, 14, 2963–2987, https://doi.org/10.5194/essd-14-2963-2022, 2022.

Humphries, R. S.: MARCUS ARM CN and CCN data reprocessed to remove ship exhaust influence, v2, CSIRO [data collection], https://doi.org/10.25919/ezp0-em87, 2020.

Humphries, R. S., McRobert, I. M., Ponsonby, W. A., Ward, J. P., Keywood, M. D., Loh, Z. M., Krummel, P. B., and Harnwell, J.: Identification of platform exhaust on the RV Investigator, Atmos. Meas. Tech., 12, 3019–3038, https://doi.org/10.5194/amt-12-3019-2019, 2019.

Humphries, R. S., McRobert, I., Ward, J., Harnwell, J., and Keywood, M. D.: CAPRICORN2 – Atmospheric aerosol measurements from the RV Investigator voyage IN2018_V01, CSIRO [data collection], https://doi.org/10.25919/2h1c-t753, 2020a.

Humphries, R. S., Simmons, J. B., McRobert, I., Ward, J., Keywood, M., Chambers, S., Griffiths, A., Williams, A. G., and Wilson, S. R.: Polar Cell Aerosol Nucleation – atmospheric measurements from the RV Investigator voyage IN2017_V01, CSIRO [data set], https://doi.org/10.25919/xs0b-an24, 2020b.

Humphries, R. S., Keywood, M. D., Gribben, S., McRobert, I. M., Ward, J. P., Selleck, P., Taylor, S., Harnwell, J., Flynn, C., Kulkarni, G. R., Mace, G. G., Protat, A., Alexander, S. P., and McFarquhar, G.: Southern Ocean latitudinal gradients of cloud condensation nuclei, Atmos. Chem. Phys., 21, 12757–12782, https://doi.org/10.5194/acp-21-12757-2021, 2021a.

Humphries, R. S., Ward, J., Keywood, M. D., and Alexander, S. P.: Atmospheric aerosol and Cloud Condensation Nuclei concentrations from Macquarie Island from 2016 to 2018, v2, CSIRO [data collection], https://doi.org/10.25919/g7jx-k629, 2021b.

Humphries, R. S., Alroe, J., Ristovski, Z., Keywood, M. D., Ward, J., McRobert, I., Cravigan, L., and Brown, R.: Aerosol Properties, Ice-edge to Equator voyage (IN2016_V03): CN3 and CCN, CSIRO [data collection], https://doi.org/10.25919/g07r-b187, 2022a.

Humphries, R. S., Alroe, J., Ward, J., Keywood, M. D., McRobert, I., Cravigan, L., and Ristovsky, Z.: Aerosol Properties, Cold Water Trial voyage (IN2015_E01): CN3 and CCN, v1, CSIRO [data collection], https://doi.org/10.25919/ytsw-9610, 2022b.

Humphries, R. S., Keywood, M. D., Ward, J. P., Harnwell, J., Alexander, S. P., Klekociuk, A. R., Hara, K., McRobert, I. M., Protat, A., Alroe, J., Cravigan, L. T., Miljevic, B., Ristovski, Z. D., Schofield, R., Wilson, S. R., Flynn, C. J., Kulkarni, G. R., Mace, G. G., McFarquhar, G. M., Chambers, S. D., Williams, A. G., and Griffiths, A. D.: Measurement report: Understanding the seasonal cycle of Southern Ocean aerosols, Atmos. Chem. Phys., 23, 3749–3777, https://doi.org/10.5194/acp-23-3749-2023, 2023.

Jaeglé, L., Quinn, P. K., Bates, T. S., Alexander, B., and Lin, J.-T.: Global distribution of sea salt aerosols: new constraints from in situ and remote sensing observations, Atmos. Chem. Phys., 11, 3137–3157, https://doi.org/10.5194/acp-11-3137-2011, 2011.

Kang, L., Marchand, R. T., Wood, R., and McCoy, I. L.: Coalescence Scavenging Drives Droplet Number Concentration in Southern Ocean Low Clouds, Geophysical Research Letters, 49, https://doi.org/10.1029/2022GL097819, 2022.

Kang, L., Marchand, R., Ma, P. L., Huang, M., Wood, R., Jongebloed, U., and Alexander, B.: Impacts of DMS Emissions and Chemistry on E3SMv2 Simulated Cloud Droplet Numbers and Aerosol Concentrations Over the Southern Ocean, Journal of Advances in Modeling Earth Systems, 17, e2024MS004683, https://doi.org/10.1029/2024MS004683, 2025.

Kettle, A. J., Andreae, M. O., Amouroux, D., Andreae, T. W., Bates, T. S., Berresheim, H., Bingemer, H., Boniforti, R., Curran, M. A. J., DiTullio, G. R., Helas, G., Jones, G. B., Keller, M. D., Kiene, R. P., Leck, C., Levasseur, M., Malin, G., Maspero, M., Matrai, P., McTaggart, A. R., Mihalopoulos, N., Nguyen, B. C., Novo, A., Putaud, J. P., Rapsomanikis, S., Roberts, G., Schebeske, G., Sharma, S., Simó, R., Staubes, R., Turner, S., and Uher, G.: A global database of sea surface dimethylsulfide (DMS) measurements and a procedure to predict sea surface DMS as a function of latitude, longitude, and month, Global Biogeochemical Cycles, 13, 399–444, https://doi.org/10.1029/1999GB900004, 1999.

Keywood, M. D., Ward, J., and Derek, N.: Cloud Condensation Nuclei Number Concentration, World Data Centre for Aerosols [data set], https://ebas-data.nilu.no/ (last access: 16 March 2023), 2023a.

Keywood, M. D., Ward, J., and Derek, N.: Particle Number Concentration, World Data Centre for Aerosols [data set], https://ebas-data.nilu.no (last access: 16 March 2023), 2023b.

Kirkby, J., Duplissy, J., Sengupta, K., Frege, C., Gordon, H., Williamson, C., Heinritzi, M., Simon, M., Yan, C., Almeida, J., Trostl, J., Nieminen, T., Ortega, I. K., Wagner, R., Adamov, A., Amorim, A., Bernhammer, A. K., Bianchi, F., Breitenlechner, M., Brilke, S., Chen, X., Craven, J., Dias, A., Ehrhart, S., Flagan, R. C., Franchin, A., Fuchs, C., Guida, R., Hakala, J., Hoyle, C. R., Jokinen, T., Junninen, H., Kangasluoma, J., Kim, J., Krapf, M., Kurten, A., Laaksonen, A., Lehtipalo, K., Makhmutov, V., Mathot, S., Molteni, U., Onnela, A., Perakyla, O., Piel, F., Petaja, T., Praplan, A. P., Pringle, K., Rap, A., Richards, N. A., Riipinen, I., Rissanen, M. P., Rondo, L., Sarnela, N., Schobesberger, S., Scott, C. E., Seinfeld, J. H., Sipila, M., Steiner, G., Stozhkov, Y., Stratmann, F., Tomé, A., Virtanen, A., Vogel, A. L., Wagner, A. C., Wagner, P. E., Weingartner, E., Wimmer, D., Winkler, P. M., Ye, P., Zhang, X., Hansel, A.,

Dommen, J., Donahue, N. M., Worsnop, D. R., Baltensperger, U., Kulmala, M., Carslaw, K. S., and Curtius, J.: Ion-induced nucleation of pure biogenic particles, Nature, 533, 521–526, https://doi.org/10.1038/nature17953, 2016.

Kiss, A. E., Hogg, A. McC., Hannah, N., Boeira Dias, F., Brassington, G. B., Chamberlain, M. A., Chapman, C., Dobrohotoff, P., Domingues, C. M., Duran, E. R., England, M. H., Fiedler, R., Griffies, S. M., Heerdegen, A., Heil, P., Holmes, R. M., Klocker, A., Marsland, S. J., Morrison, A. K., Munroe, J., Nikurashin, M., Oke, P. R., Pilo, G. S., Richet, O., Savita, A., Spence, P., Stewart, K. D., Ward, M. L., Wu, F., and Zhang, X.: ACCESS-OM2 v1.0: a global ocean–sea ice model at three resolutions, Geosci. Model Dev., 13, 401–442, https://doi.org/10.5194/gmd-13-401-2020, 2020.

Korhonen, P., Kulmala, M., Laaksonen, A., Viisanen, Y., McGraw, R., and Seinfeld, J. H.: Ternary nucleation of H_2SO_4, NH_3, and H_2O in the atmosphere, Journal of Geophysical Research Atmospheres, 104, 26349–26353, https://doi.org/10.1029/1999jd900784, 1999.

Kulmala, M., Laaksonen, A., and Pirjola, L.: Parameterizations for sulfuric acid/water nucleation rates, Journal of Geophysical Research, 103, 8301, https://doi.org/10.1029/97JD03718, 1998.

Lana, A., Bell, T. G., Simó, R., Vallina, S. M., Ballabrera-Poy, J., Kettle, A. J., Dachs, J., Bopp, L., Saltzman, E. S., Stefels, J., Johnson, J. E., and Liss, P. S.: An updated climatology of surface dimethlysulfide concentrations and emission fluxes in the global ocean, Global Biogeochemical Cycles, 25, https://doi.org/10.1029/2010GB003850, 2011.

Lannuzel, D., Wongpan, P., Hayashida, H., and Burke, G.: A data collation for climate-cooling gas dimethylsulphide in Antarctic snow, sea ice and underlying seawater, Ver. 1, Australian Antarctic Data Centre, https://doi.org/10.26179/svxw-kt31, 2024.

Lee, S., Gordon, H., Yu, H., Lehtipalo, K., Haley, R., Li, Y., and Zhang, R.: New Particle Formation in the Atmosphere: From Molecular Clusters to Global Climate, Journal of Geophysical Research: Atmospheres, 124, 7098–7146, https://doi.org/10.1029/2018JD029356, 2019.

Liss, P. S. and Merlivat, L.: Air-Sea Gas Exchange Rates: Introduction and Synthesis, in: The Role of Air-Sea Exchange in Geochemical Cycling, edited by: Buat-Ménard, P., 113–127, Springer Netherlands, Dordrecht, https://doi.org/10.1007/978-94-009-4738-2_5, 1986.

Mace, G. G., Benson, S., Sterner, E., Protat, A., Humphries, R., and Hallar, A. G.: The Association Between Cloud Droplet Number over the Summer Southern Ocean and Air Mass History, Journal of Geophysical Research: Atmospheres, 129, https://doi.org/10.1029/2023JD040673, 2024.

Mallet, M. D., Cravigan, L. T., Milic, A., Alroe, J., Ristovski, Z. D., Ward, J., Keywood, M., Williams, L. R., Selleck, P., and Miljevic, B.: Composition, size and cloud condensation nuclei activity of biomass burning aerosol from northern Australian savannah fires, Atmos. Chem. Phys., 17, 3605–3617, https://doi.org/10.5194/acp-17-3605-2017, 2017.

Mallet, M. D., Humphries, R. S., Fiddes, S. L., Alexander, S. P., Altieri, K., Angot, H., Anilkumar, N., Bartels-Rausch, T., Creamean, J., Dall'Osto, M., Dommergue, A., Frey, M., Henning, S., Lannuzel, D., Lapere, R., Mace, G. G., Mahajan, A. S., McFarquhar, G. M., Meiners, K. M., Miljevic, B., Peeken, I., Protat, A., Schmale, J., Steiner, N., Sellegri, K., Simó, R., Thomas, J. L., Willis, M. D., Winton, V. H. L., and Woodhouse, M. T.: Untangling the influence of Antarctic and Southern Ocean life on clouds, Elementa: Science of the Anthropocene, 11, https://doi.org/10.1525/elementa.2022.00130, 2023.

Mallet, M. D., Miljevic, B., Humphries, R. S., Mace, G. G., Alexander, S. P., Protat, A., Chambers, S., Cravigan, L., DeMott, P. J., Fiddes, S., Harnwell, J., Keywood, M. D., McFarquhar, G. M., McRobert, I., Moore, K. A., Mynard, C., Osuagwu, C. G., Ristovski, Z., Selleck, P., Taylor, S., Ward, J., and Williams, A.: Biological enhancement of cloud droplet concentrations observed off East Antarctica, npj Climate and Atmospheric Science, 8, 1–7, https://doi.org/10.1038/S41612-025-00990-5, 2025.

Mann, G. W., Carslaw, K. S., Spracklen, D. V., Ridley, D. A., Manktelow, P. T., Chipperfield, M. P., Pickering, S. J., and Johnson, C. E.: Description and evaluation of GLOMAP-mode: a modal global aerosol microphysics model for the UKCA composition-climate model, Geosci. Model Dev., 3, 519–551, https://doi.org/10.5194/gmd-3-519-2010, 2010.

Mann, G. W., Carslaw, K. S., Ridley, D. A., Spracklen, D. V., Pringle, K. J., Merikanto, J., Korhonen, H., Schwarz, J. P., Lee, L. A., Manktelow, P. T., Woodhouse, M. T., Schmidt, A., Breider, T. J., Emmerson, K. M., Reddington, C. L., Chipperfield, M. P., and Pickering, S. J.: Intercomparison of modal and sectional aerosol microphysics representations within the same 3-D global chemical transport model, Atmos. Chem. Phys., 12, 4449–4476, https://doi.org/10.5194/acp-12-4449-2012, 2012.

Marchand, R.: Macquarie Island Cloud and Radiation Experiment (MICRE) Field Campaign Report, Tech. rep., Atmospheric Radiation Measurement (ARM) Archive, Oak Ridge National Laboratory (ORNL), Oak Ridge, TN (US), https://doi.org/10.2172/1602536, 2020.

McCluskey, C. S., Hill, T. C. J., Malfatti, F., Sultana, C. M., Lee, C., Santander, M. V., Beall, C. M., Moore, K. A., Cornwell, G. C., Collins, D. B., Prather, K. A., Jayarathne, T., Stone, E. A., Azam, F., Kreidenweis, S. M., and DeMott, P. J.: A Dynamic Link between Ice Nucleating Particles Released in Nascent Sea Spray Aerosol and Oceanic Biological Activity during Two Mesocosm Experiments, Journal of the Atmospheric Sciences, 74, 151–166, https://doi.org/10.1175/JAS-D-16-0087.1, 2017.

McCluskey, C. S., Hill, T. C., Humphries, R. S., Rauker, A. M., Moreau, S., Strutton, P. G., Chambers, S. D., Williams, A. G., McRobert, I., Ward, J., Keywood, M. D., Harnwell, J., Ponsonby, W., Loh, Z. M., Krummel, P. B., Protat, A., Kreidenweis, S. M., and DeMott, P. J.: Observations of Ice Nucleating Particles Over Southern Ocean Waters, Geophysical Research Letters, 45, 989–11, https://doi.org/10.1029/2018GL079981, 2018.

McCluskey, C. S., Gettelman, A., Bardeen, C. G., DeMott, P. J., Moore, K. A., Kreidenweis, S. M., Hill, T. C., Barry, K. R., Twohy, C. H., Toohey, D. W., Rainwater, B., Jensen, J. B., Reeves, J. M., Alexander, S. P., and McFarquhar, G. M.: Simulating Southern Ocean Aerosol and Ice Nucleating Particles in the Community Earth System Model Version 2, Journal of Geophysical Research: Atmospheres, 128, https://doi.org/10.1029/2022JD036955, 2023.

McCormick, R. A. and Ludwig, J. H.: Climate Modification by Atmospheric Aerosols, Science, 156, 1358–1359, https://doi.org/10.1126/science.156.3780.1358, 1967.

McCoy, I. L., Bretherton, C. S., Wood, R., Twohy, C. H., Gettelman, A., Bardeen, C. G., and Toohey, D. W.: Influences of Re-

cent Particle Formation on Southern Ocean Aerosol Variability and Low Cloud Properties, Journal of Geophysical Research: Atmospheres, 126, https://doi.org/10.1029/2020JD033529, 2021.

McFarquhar, G. M., Bretherton, C. S., Marchand, R., Protat, A., DeMott, P. J., Alexander, S. P., Roberts, G. C., Twohy, C. H., Toohey, D., Siems, S., Huang, Y., Wood, R., Rauber, R. M., Lasher-Trapp, S., Jensen, J., Stith, J. L., Mace, J., Um, J., Järvinen, E., Schnaiter, M., Gettelman, A., Sanchez, K. J., McCluskey, C. S., Russell, L. M., McCoy, I. L., Atlas, R. L., Bardeen, C. G., Moore, K. A., Hill, T. C. J., Humphries, R. S., Keywood, M. D., Ristovski, Z., Cravigan, L., Schofield, R., Fairall, C., Mallet, M. D., Kreidenweis, S. M., Rainwater, B., D'Alessandro, J., Wang, Y., Wu, W., Saliba, G., Levin, E. J. T., Ding, S., Lang, F., Truong, S. C. H., Wolff, C., Haggerty, J., Harvey, M. J., Klekociuk, A. R., and McDonald, A.: Observations of Clouds, Aerosols, Precipitation, and Surface Radiation over the Southern Ocean: An Overview of CAPRICORN, MARCUS, MICRE, and SOCRATES, Bulletin of the American Meteorological Society, 102, E894–E928, https://doi.org/10.1175/BAMS-D-20-0132.1, 2021.

Merikanto, J., Spracklen, D. V., Mann, G. W., Pickering, S. J., and Carslaw, K. S.: Impact of nucleation on global CCN, Atmos. Chem. Phys., 9, 8601–8616, https://doi.org/10.5194/acp-9-8601-2009, 2009.

Metzger, A., Verheggen, B., Dommen, J., Duplissy, J., Prevot, A. S. H., Weingartner, E., Riipinen, I., Kulmala, M., Spracklen, D. V., Carslaw, K. S., and Baltensperger, U.: Evidence for the role of organics in aerosol particle formation under atmospheric conditions, Proceedings of the National Academy of Sciences of the United States of America, 107, 6646–6651, https://doi.org/10.1073/pnas.0911330107, 2010.

Modini, R. L., Ristovski, Z. D., Johnson, G. R., He, C., Surawski, N., Morawska, L., Suni, T., and Kulmala, M.: New particle formation and growth at a remote, sub-tropical coastal location, Atmos. Chem. Phys., 9, 7607–7621, https://doi.org/10.5194/acp-9-7607-2009, 2009.

Mulcahy, J. P., Jones, C., Sellar, A., Johnson, B., Boutle, I. A., Jones, A., Andrews, T., Rumbold, S. T., Mollard, J., Bellouin, N., Johnson, C. E., Williams, K. D., Grosvenor, D. P., and McCoy, D. T.: Improved Aerosol Processes and Effective Radiative Forcing in HadGEM3 and UKESM1, Journal of Advances in Modeling Earth Systems, 10, 2786–2805, https://doi.org/10.1029/2018MS001464, 2018.

Mulcahy, J. P., Johnson, C., Jones, C. G., Povey, A. C., Scott, C. E., Sellar, A., Turnock, S. T., Woodhouse, M. T., Abraham, N. L., Andrews, M. B., Bellouin, N., Browse, J., Carslaw, K. S., Dalvi, M., Folberth, G. A., Glover, M., Grosvenor, D. P., Hardacre, C., Hill, R., Johnson, B., Jones, A., Kipling, Z., Mann, G., Mollard, J., O'Connor, F. M., Palmiéri, J., Reddington, C., Rumbold, S. T., Richardson, M., Schutgens, N. A. J., Stier, P., Stringer, M., Tang, Y., Walton, J., Woodward, S., and Yool, A.: Description and evaluation of aerosol in UKESM1 and HadGEM3-GC3.1 CMIP6 historical simulations, Geosci. Model Dev., 13, 6383–6423, https://doi.org/10.5194/gmd-13-6383-2020, 2020.

Oke, P. R., Griffin, D. A., Schiller, A., Matear, R. J., Fiedler, R., Mansbridge, J., Lenton, A., Cahill, M., Chamberlain, M. A., and Ridgway, K.: Evaluation of a near-global eddy-resolving ocean model, Geosci. Model Dev., 6, 591–615, https://doi.org/10.5194/gmd-6-591-2013, 2013.

Paulot, F., Paynter, D., Winton, M., Ginoux, P., Zhao, M., and Horowitz, L. W.: Revisiting the Impact of Sea Salt on Climate Sensitivity, Geophysical Research Letters, 47, https://doi.org/10.1029/2019GL085601, 2020.

Petters, M. D. and Kreidenweis, S. M.: A single parameter representation of hygroscopic growth and cloud condensation nucleus activity, Atmos. Chem. Phys., 7, 1961–1971, https://doi.org/10.5194/acp-7-1961-2007, 2007.

Pincus, R. and Baker, M. B.: Effect of precipitation on the albedo susceptibility of clouds in the marine boundary layer, Nature, 372, 250–252, https://doi.org/10.1038/372250a0, 1994.

Prather, K. A., Bertram, T. H., Grassian, V. H., Deane, G. B., Stokes, M. D., DeMott, P. J., Aluwihare, L. I., Palenik, B. P., Azam, F., Seinfeld, J. H., Moffet, R. C., Molina, M. J., Cappa, C. D., Geiger, F. M., Roberts, G. C., Russell, L. M., Ault, A. P., Baltrusaitis, J., Collins, D. B., Corrigan, C. E., Cuadra-Rodriguez, L. A., Ebben, C. J., Forestieri, S. D., Guasco, T. L., Hersey, S. P., Kim, M. J., Lambert, W. F., Modini, R. L., Mui, W., Pedler, B. E., Ruppel, M. J., Ryder, O. S., Schoepp, N. G., Sullivan, R. C., and Zhao, D.: Bringing the ocean into the laboratory to probe the chemical complexity of sea spray aerosol, Proceedings of the National Academy of Sciences of the United States of America, 110, 7550–7555, https://doi.org/10.1073/pnas.1300262110, 2013.

Protat, A.: RV Investigator BOM Atmospheric Data Overview (2016 onwards), CSIRO [data collection], https://doi.org/10.25919/5f688fcc97166, 2020.

Protat, A., Schulz, E., Rikus, L., Sun, Z., Xiao, Y., and Keywood, M. D.: Shipborne observations of the radiative effect of Southern Ocean clouds, Journal of Geophysical Research: Atmospheres, 122, 318–328, https://doi.org/10.1002/2016JD026061, 2017.

Quinn, P. K. and Bates, T. S.: The case against climate regulation via oceanic phytoplankton sulphur emissions, Nature, 480, 51–56, https://doi.org/10.1038/nature10580, 2011.

Quinn, P. K., Collins, D. B., Grassian, V. H., Prather, K. A., and Bates, T. S.: Chemistry and Related Properties of Freshly Emitted Sea Spray Aerosol, Chem. Rev., 115, 4383–4399, https://doi.org/10.1021/cr500713g, 2015.

Regayre, L. A., Schmale, J., Johnson, J. S., Tatzelt, C., Baccarini, A., Henning, S., Yoshioka, M., Stratmann, F., Gysel-Beer, M., Grosvenor, D. P., and Carslaw, K. S.: The value of remote marine aerosol measurements for constraining radiative forcing uncertainty, Atmos. Chem. Phys., 20, 10063–10072, https://doi.org/10.5194/acp-20-10063-2020, 2020.

Revell, L. E., Kremser, S., Hartery, S., Harvey, M., Mulcahy, J. P., Williams, J., Morgenstern, O., McDonald, A. J., Varma, V., Bird, L., and Schuddeboom, A.: The sensitivity of Southern Ocean aerosols and cloud microphysics to sea spray and sulfate aerosol production in the HadGEM3-GA7.1 chemistry–climate model, Atmos. Chem. Phys., 19, 15447–15466, https://doi.org/10.5194/acp-19-15447-2019, 2019.

Revell, L. E., Wotherspoon, N. E., Jones, O. J., Bhatti, Y. A., Williams, J. H. T., Mackie, S. L., and Mulcahy, J. P.: Atmosphere-Ocean Feedback From Wind-Driven Sea Spray Aerosol Production, Geophysical Research Letters, 48, https://doi.org/10.1029/2020GL091900, 2021.

Rodríguez-Ros, P., Galí, M., Cortés, P., Robinson, C. M., Antoine, D., Wohl, C., Yang, M. X., and Simó, R.: Remote Sensing Retrieval of Isoprene Concentrations in

the Southern Ocean, Geophysical Research Letters, 47, https://doi.org/10.1029/2020GL087888, 2020.

Russell, L. M., Moore, R. H., Burrows, S. M., and Quinn, P. K.: Ocean flux of salt, sulfate, and organic components to atmospheric aerosol, Earth-Science Reviews, 239, 104364, https://doi.org/10.1016/j.earscirev.2023.104364, 2023.

Schmale, J., Baccarini, A., Thurnherr, I., Henning, S., Efraim, A., Regayre, L., Bolas, C., Hartmann, M., Welti, A., Lehtipalo, K., Aemisegger, F., Tatzelt, C., Landwehr, S., Modini, R. L., Tummon, F., Johnson, J. S., Harris, N., Schnaiter, M., Toffoli, A., Derkani, M., Bukowiecki, N., Stratmann, F., Dommen, J., Sperger, U. B., Wernli, H., Rosenfeld, D., Gysel-Beer, M., and Carslaw, K. S.: Overview of the antarctic circumnavigation expedition: Study of preindustrial-like aerosols and their climate effects (ACE-SPACE), Bulletin of the American Meteorological Society, 100, 2260–2283, https://doi.org/10.1175/BAMS-D-18-0187.1, 2019.

Schofield, R. and Ryan, R.: Observations collected between 18th October 2018 and 29th March 2019 aboard Aurora Australis by AIRBOX and associated instruments, Ver. 1, CSIRO [data collection], https://doi.org/10.26179/5e546f452145d, 2021.

Schuddeboom, A. J. and McDonald, A. J.: The Southern Ocean Radiative Bias, Cloud Compensating Errors, and Equilibrium Climate Sensitivity in CMIP6 Models, Journal of Geophysical Research: Atmospheres, 126, https://doi.org/10.1029/2021JD035310, 2021.

Schutgens, N., Tsyro, S., Gryspeerdt, E., Goto, D., Weigum, N., Schulz, M., and Stier, P.: On the spatio-temporal representativeness of observations, Atmos. Chem. Phys., 17, 9761–9780, https://doi.org/10.5194/acp-17-9761-2017, 2017.

Sellegri, K., Barthelmeß, T., Trueblood, J., Cristi, A., Freney, E., Rose, C., Barr, N., Harvey, M., Safi, K., Deppeler, S., Thompson, K., Dillon, W., Engel, A., and Law, C.: Quantified effect of seawater biogeochemistry on the temperature dependence of sea spray aerosol fluxes, Atmos. Chem. Phys., 23, 12949–12964, https://doi.org/10.5194/acp-23-12949-2023, 2023.

Simmons, J. B., Humphries, R. S., Wilson, S. R., Chambers, S. D., Williams, A. G., Griffiths, A. D., McRobert, I. M., Ward, J. P., Keywood, M. D., and Gribben, S.: Summer aerosol measurements over the East Antarctic seasonal ice zone, Atmos. Chem. Phys., 21, 9497–9513, https://doi.org/10.5194/acp-21-9497-2021, 2021.

Stephens, G. L., L'Ecuyer, T., Forbes, R., Gettelmen, A., Golaz, J.-C., Bodas-Salcedo, A., Suzuki, K., Gabriel, P., and Haynes, J.: Dreary state of precipitation in global models, Journal of Geophysical Research: Atmospheres, 115, https://doi.org/10.1029/2010JD014532, 2010.

Telford, P. J., Braesicke, P., Morgenstern, O., and Pyle, J. A.: Technical Note: Description and assessment of a nudged version of the new dynamics Unified Model, Atmos. Chem. Phys., 8, 1701–1712, https://doi.org/10.5194/acp-8-1701-2008, 2008.

Trevena, A. and Jones, G.: DMS flux over the Antarctic sea ice zone, Marine Chemistry, 134–135, 47–58, https://doi.org/10.1016/j.marchem.2012.03.001, 2012.

Twomey, S.: Pollution and the Planetary Albedo, Atmospheric Environment, 8, 1251–1256, 1974.

Uhe, P. and Thatcher, M.: A spectral nudging method for the ACCESS1.3 atmospheric model, Geosci. Model Dev., 8, 1645–1658, https://doi.org/10.5194/gmd-8-1645-2015, 2015.

Uin, J., Aiken, A. C., Dubey, M. K., Kuang, C., Pekour, M., Salwen, C., Sedlacek, A. J., Senum, G., Smith, S., Wang, J., Watson, T. B., and Springston, S. R.: Atmospheric radiation measurement (ARM) aerosol observing systems (AOS) for surface-based in situ atmospheric aerosol and trace gas measurements, Journal of Atmospheric and Oceanic Technology, 36, 2429–2447, https://doi.org/10.1175/JTECH-D-19-0077.1, 2019.

van Marle, M. J. E., Kloster, S., Magi, B. I., Marlon, J. R., Daniau, A.-L., Field, R. D., Arneth, A., Forrest, M., Hantson, S., Kehrwald, N. M., Knorr, W., Lasslop, G., Li, F., Mangeon, S., Yue, C., Kaiser, J. W., and van der Werf, G. R.: Historic global biomass burning emissions for CMIP6 (BB4CMIP) based on merging satellite observations with proxies and fire models (1750–2015), Geosci. Model Dev., 10, 3329–3357, https://doi.org/10.5194/gmd-10-3329-2017, 2017.

Venugopal, A. U., Bhatti, Y. A., Morgenstern, O., Williams, J., Edkins, N., Hardacre, C., Jones, A., and Revell, L. E.: Constraining the Uncertainty Associated With Sea Salt Aerosol Parameterizations in Global Models Using Nudged UKESM1-AMIP Simulations, Journal of Geophysical Research: Atmospheres, 130, e2024JD041643, https://doi.org/10.1029/2024JD041643, 2025.

Vergara-Temprado, J., Miltenberger, A. K., Furtado, K., Grosvenor, D. P., Shipway, B. J., Hill, A. A., Wilkinson, J. M., Field, P. R., Murray, B. J., and Carslaw, K. S.: Strong control of Southern Ocean cloud reflectivity by ice-nucleating particles, Proceedings of the National Academy of Sciences of the United States of America, 115, 2687–2692, https://doi.org/10.1073/pnas.1721627115, 2018.

Vignon, E., Alexander, S. P., DeMott, P. J., Sotiropoulou, G., Gerber, F., Hill, T. C. J., Marchand, R., Nenes, A., and Berne, A.: Challenging and Improving the Simulation of Mid-Level Mixed-Phase Clouds Over the High-Latitude Southern Ocean, Journal of Geophysical Research: Atmospheres, 126, https://doi.org/10.1029/2020JD033490, 2021.

Vlahos, P. and Monahan, E. C.: A generalized model for the air-sea transfer of dimethyl sulfide at high wind speeds, Geophysical Research Letters, 36, L21605, https://doi.org/10.1029/2009GL040695, 2009.

Walters, D., Baran, A. J., Boutle, I., Brooks, M., Earnshaw, P., Edwards, J., Furtado, K., Hill, P., Lock, A., Manners, J., Morcrette, C., Mulcahy, J., Sanchez, C., Smith, C., Stratton, R., Tennant, W., Tomassini, L., Van Weverberg, K., Vosper, S., Willett, M., Browse, J., Bushell, A., Carslaw, K., Dalvi, M., Essery, R., Gedney, N., Hardiman, S., Johnson, B., Johnson, C., Jones, A., Jones, C., Mann, G., Milton, S., Rumbold, H., Sellar, A., Ujiie, M., Whitall, M., Williams, K., and Zerroukat, M.: The Met Office Unified Model Global Atmosphere 7.0/7.1 and JULES Global Land 7.0 configurations, Geosci. Model Dev., 12, 1909–1963, https://doi.org/10.5194/gmd-12-1909-2019, 2019.

Wang, W.-L., Song, G., Primeau, F., Saltzman, E. S., Bell, T. G., and Moore, J. K.: Global ocean dimethyl sulfide climatology estimated from observations and an artificial neural network, Biogeosciences, 17, 5335–5354, https://doi.org/10.5194/bg-17-5335-2020, 2020.

Watson-Parris, D. and Smith, C. J.: Large uncertainty in future warming due to aerosol forcing, Nature Climate Change, 12, 1111–1113, https://doi.org/10.1038/s41558-022-01516-0, 2022.

Webb, A. L., van Leeuwe, M. A., den Os, D., Meredith, M. P., Venables, J. H., and Stefels, J.: Extreme spikes in DMS flux

double estimates of biogenic sulfur export from the Antarctic coastal zone to the atmosphere, Scientific Reports, 9, https://doi.org/10.1038/s41598-019-38714-4, 2019.

Woodward, S.: Modeling the atmospheric life cycle and radiative impact of mineral dust in the Hadley Centre climate model, Journal of Geophysical Research: Atmospheres, 106, 18155–18166, https://doi.org/10.1029/2000JD900795, 2001.

World Meteorological Organization (WMO): WMO/GAW Aerosol Measurement Procedures, Guidelines and Recommendations, WMO, Geneva, 2nd edn., https://library.wmo.int/idurl/4/55277 (last access: 17 January 2024), 2016.

Yu, Z. and Li, Y.: Marine volatile organic compounds and their impacts on marine aerosol – A review, Science of The Total Environment, 768, 145054, https://doi.org/10.1016/J.SCITOTENV.2021.145054, 2021.

Zelinka, M. D., Myers, T. A., McCoy, D. T., Po-Chedley, S., Caldwell, P. M., Ceppi, P., Klein, S. A., and Taylor, K. E.: Causes of Higher Climate Sensitivity in CMIP6 Models, Geophysical Research Letters, 47, 1–12, https://doi.org/10.1029/2019GL085782, 2020.

Zhou, S., Chen, Y., Huang, S., Gong, X., Yang, G., Zhang, H., Herrmann, H., Wiedensohler, A., Poulain, L., Zhang, Y., Wang, F., Xu, Z., and Yan, K.: A 20-year (1998–2017) global sea surface dimethyl sulfide gridded dataset with daily resolution, Earth Syst. Sci. Data, 16, 4267–4290, https://doi.org/10.5194/essd-16-4267-2024, 2024.